Deliverable Number D3.4: Technical report on the CO_2 storage site Sleipner; WP3; lead beneficiary number 5 (UiB)

Sub-seabed CO_2 Storage: Impact on Marine Ecosystems

Technical report on environmental conditions and possible leak scenarios in the North Sea.

Authors: Guttorm Alendal[1], Marius Dewar[2], Alfatih Ali[1], Yakushev Evgeniy[3], Lisa Vielstädte[4], Helge Avlesen[5], Baixin Chen[2].

[1]Department of Mathematics, University of Bergen, Bergen, Norway

[2]Institute of Mechanical, Process and Energy Engineering, Heriot-Watt University Edinburgh, UK

[3]NIVA, Norwegian Institute for Water Research, Oslo, Norway

[4]Helmholtz Zentrum für Ozeanforschung Kiel GEOMAR Kiel, Germany.

[5]Uni Computing, Bergen, Norway

Contents

Executive summary and conclusions

This report documents the leak scenarios that have been simulated within WP3 as part of the overall scenarios as defined under the CCT2 umbrella. The likelihood of the different scenarios will be addressed in WP1 and WP2, in WP3 the objective is to estimate the spatial footprint of a leak, and how much acidification is to be expected. Subsequent environmental impact assessments are the scope of WP4.

Within WP3 there are three classes of models; a marine chemistry model, two different Near-field two-phase plume models, NFTPM, and a regional scale general circulation model (BOM, Bergen Ocean Model). They all have different needs with regards to data for calibration and validation. The models are all described in depth in ECO2 D3.3 (Dewar et al. 2013) including a general discussion on model parameters.

The spatial (temporal) scales of the model framework used within WP3 cover the spatial (temporal) ranges from 10^{-2} m (minutes) of biogeochemical transfer and leaked bubble dynamics; through 10^{3} m (hours to days) of the near-field plume and acute impacts (Near-field two-phase plume model, NFTPM); to $10^{6} \sim 10^{7}$ m (weeks to months) of leaked CO_2 dispersion and transport in North Sea (Bergen Ocean Model (BOM)). This is a challenge; they have different needs with respect to input parameters and gives different results.

Even though the models used in this study are very different they all indicate that the footprint of a leak will be very localized in the vicinity of a leak. Not surprisingly, the flux of CO_2 governs how much the maximum concentration will become, and the spatial extent of the footprint. The topology of the leak (dispersed leaks over an area vs. large flux at a point) also influences, the same does size distribution of the seep. Hence, proper and reliable predictions on how the CO_2 reaches the seafloor is important in order to estimate the spatial and temporal footprint of a leak.

Local stratification and current conditions have little influence on the vertical movement and dissolution of bubbles. Hence, low impact on the vertical distribution of the seeped CO_2 in the water column. But, once dissolved into the seawater further transport and dilution of the CO_2 content is highly dependent on local stratification and current

conditions, including small scale turbulent mixing. Strong currents will bring the CO_2 cloud over a larger distance in less time, on the other hand strong currents usually implies higher shear, at least along the seafloor, and hence stronger turbulent mixing. The varying current direction also determines the bearing taken by the CO_2 cloud. Even though mean signal will be very low when moving a distance away from the seep patches of higher concentration my pass

The marine environment is not stagnant and varies due to tides, seasons and storm surges. Proper statistics and understanding of the local conditions will lay the foundation for predicting how the CO_2 signal can be distinguished from natural CO_2 content. Natural variability in, and possible general acidification of, the oceans CO_2 concentration will govern our ability to detect any changes and the potential extra stress imposed on the environment. As long as the signal stays below natural variability it will be extremely hard to distinguish impacts and to detect, localize and quantify a leak.
The small spatial footprint expected from a CO_2 seep should indicate very localized potential environmental impacts. On the other hand it will make detecting and localizing a leak a bigger challenge.

Introduction, motivation and background

Modelling the fate of CO_2 seeped through the seafloor will be important in many aspects during planning, operational, and closure phases of a sub-sea geological storage project. How the leaked CO_2 is transported and diluted in the water masses will influence on the magnitude of the spatial and temporal environmental footprint a leak might impose. Increased CO_2 concentration leads to acidification of the water masses that might cause impact on the marine ecosystem (Blackford et al, 2010). How far away from a leak it is detectable will influence on the design of a monitoring program. Further, how local currents transport, and dilute; the CO_2 will determine whether it might reach the surface and subsequent outgassing to the atmosphere.

CO_2 might reach the marine environment along many pathways. Part of leaked CO_2 might be dissolved in seafloor sediments, creating negative buoyant water parcels that will tend

to migrate in the horizontal and might accumulate in topographic depressions. An interaction between the seawater and the sediments plays an important role in the biogeochemical cycling. The benthic fluxes of chemical elements affect directly the acidification characteristics (i.e. pH and carbonate saturation) and also determine the functionality of the benthic and pelagic ecosystems. In many regions redox state of the near bottom layer can oscillate in connection with supply of organic matter (OM), physical regime and coastal discharge influence.

Pure CO_2 will be less dense than seawater at depth shallower than approx. 3500 meters, and will be in gaseous phase if shallower than 500 meters depth. Hence the most likely scenario is that a leak will create droplets (liquid) or bubble (gaseous) ascending through the water column. Since the site of study will be the Sleipner area of around 90 meters depth the focus here will be on bubbles.

As the bubbles (the dispersed phase, with size up to 20 – 30 mm) ascend the surrounding water masses (the carrier phase) there will be a two way dynamical coupling. The magnitude of influence from the dispersed phase will depend on bubbles sizes and amount of bubbles being present. The most dominant processes will be interfacial drag from individual bubbles, retarding the bubble ascent and creating a lifting force to the carrier phase. This entrained water will be lifted upward into, in case of stratification, a less dense environment. Simultaneously the CO_2 gas within the bubble will be transferred through the interface and dissolved into the surrounding water, increasing the density. Hence, the entrained water will be negatively buoyant. The combination of these processes, coupled with a dynamically active water column, creates bubbles plumes. Simulating such events is challenging, especially due to the many different scales that are involved.
The development and verification of a near field, at scales from 10^{-2} m of bubbles to 10^{3} m of the CO_2 enriched seawater plume, multiphase plume model are the integration of sub-models for plume dynamics through exchanges in momentum and mass between dispersion phase and the ambient environment (currents, temp/salinity profiles).

The local current and stratification will influence on the evolvement of the plume, variability in current direction and speed will make the spatial footprint highly time dependent. These local currents will also transport the dissolved CO_2 as a passive tracer once it has been diluted enough to make it a passive tracer. To prepare for the Sleipner scenarios the Bergen Ocean Model (BOM) has been set up for the North Sea. Tidal forcing and wind taken from spring 2012 have been used to drive the model.

Four different models have been used in the study, the biogeochemical model developed at NIVA, the Geomar bubble plume model, the HWU developed multiphase plume model, and Bergen Ocean Model being used by UiB. They all require different input, and provide different results. See ECO2 D3.3 for detailed technical descriptions of the models and preparation for the scenarios.

The leak scenarios

Through the work within ECO2 WP1 and WP2 it has been decided on two primary scenarios that we should apply to each of our model systems (1&2 below), and two more scenarios (3&4) that could be considered.

Scenario	Max flux rate (at seafloor)	Footprint (at seafloor)	Relevant Stuttgart scenario
1) Chimney reactivation	~150T/d	500m diameter circle	Snohvit Realistic Chimney 15
2) Elongated conduit (Fault/Fracture/Chimney)	~15T/d	200x2000m fracture zone	Snohvit Realistic Chimney 15
3) Blowout	~100T/d	50m diameter circle	Generic Gas Chimney 19
4) Leaky well	~20T/a	10m diameter circle	~

For each of these scenarios a time evolution of the CO_2 flux rates has been delivered as shown in Figure 1. None of the models used here has the ability to integrate forward for

years in time. Hence, the fluxes are considered constant in all the simulations, with rates being representative for the time evolution shown.

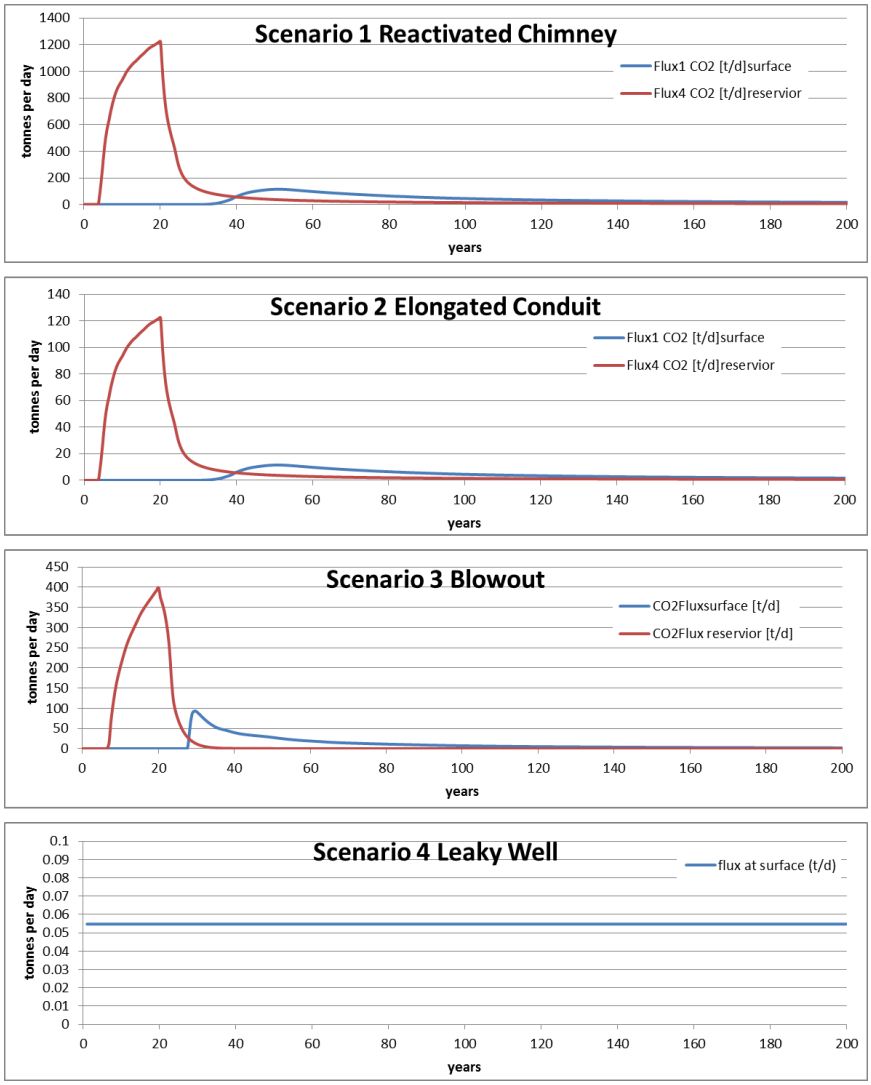

Figure 1: The time evolution of leakage fluxes for the different scenarios.

The environmental conditions in the North Sea.

As the CO_2 enters the water columns the local environment will influence on how it is transported, dissolved and diluted. Local current direction will determine the direction of transport, while high shear and small scale turbulence will increase the mixing and hence, the rate of dilution of the CO_2 signal. Especially the shear layer along the seafloor is influenced by current direction and speed, and small-scale topography.

The total carbon content in the North Sea underlies natural seasonal variability with values of 2135 µmol kg^{-1} and 2175 µmol kg^{-1} in the bottom water in winter and summer, respectively (Bozek et al., 2006). According to this and considering CTD and total alkalinity measurements in the Sleipner area, the pCO_2 varies naturally by 108.4 µatm, i.e. 381.8 to 490.2 µatm between winter and summer. Salt et al. (2013) showed coupling between CO_2 content in the North Sea and the North Atlantic Oscillation, hence changes in water masses characteristics.

As long as the signal stays below natural variability it will be hard to distinguish impacts and to detect, localize and quantify a leak. Procedures for filtering away natural variability from a signal, in order to detect small fluxes through the seafloor, have been suggested in Omar et al (2014).

The current conditions

The tidal ellipse represents an oscillatory behaviour of current amplitude and direction. Davies and Furnes (1980) analysed a number of time series in the North Sea focusing on the most energetic component the M2 semidiurnal with period 12.42 hours. Their stations 51, 52, 521, 71 are located close to the Sleipner area, while 83 and 58 lays a bit further north.

Table 1 The tidal ellipse parameters at different stations and depths. Negative minor value indicates a clockwise rotation of the ellipse from east. Only observations listed. Taken from Davies and Furnes (1980).

Station	Depth	Major	Minor	Incl
	(m)	(cm/s)	(cm/s)	Degrees
51	66	9	-1	95
	126	15	-1	85
52	59	14	-4	73
	74	19	-6	74
71	36	16	-4	99
	66	19	-5	80
	104	14	-2	85
58	55	17	-4	86
	115	11	-1	88
83	65	14	-5	97
	115	7	-1	133

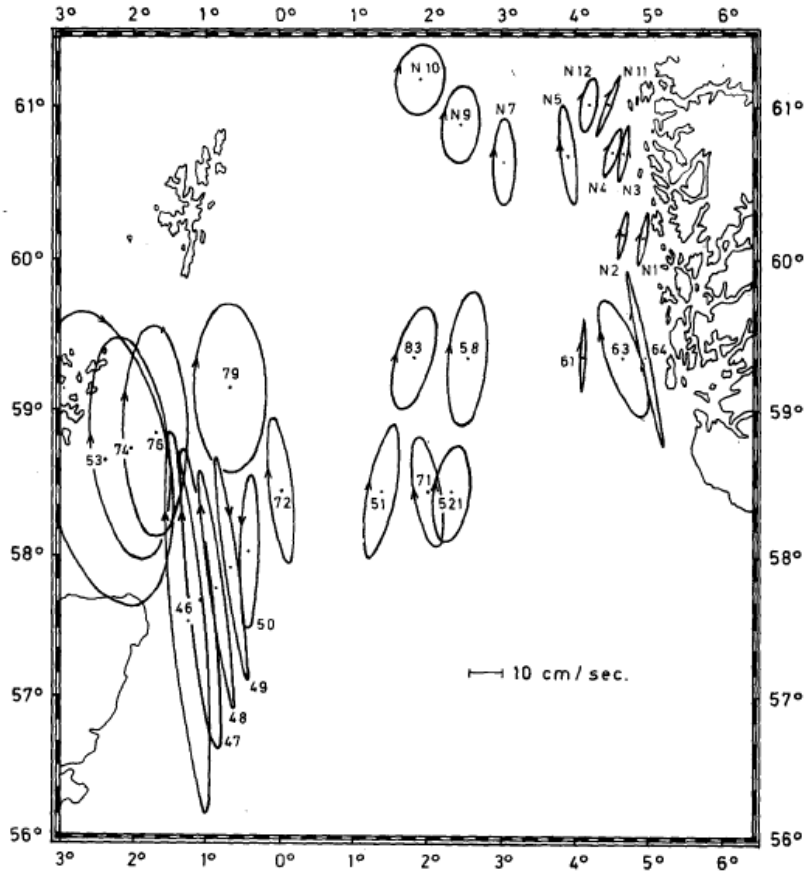

Figure 2: Surface tidal ellipses at selected stations in the North Sea, taken from Davies & Fursnes, 1980.

To supplement the tidal signal above, the tidal signal from BOM has been analysed using the free available Matlab package *t_tide* (Pawlowicz, Beardsley, & Lentz, 2002). For each depth the East and North velocities are fed to the package. The package returns ellipsis parameter for 35 components, including 95% confidence intervals, and a prediction of the current due to the tide at the same times as the original time series.

Result for the most energetic M2 component is listed in Table 2, while the vertical profile of the M2 ellipsis in the vicinity of Sleipner is shown in Figure 3. The tidal time series provided by the t_tide package allows for statistical description of the tidal signal without having to analyse each component. Performing a PCA analysis of the tidal prediction gives the similar rotation, at least within the errorbars, as in Figure 3.

Table 2 M2 ellipsis from BOM simulation at the leak location. Negative minor value indicates a clockwise rotation, with angle Inc, of the ellipse from east.

Point	Depth	Major	Minor	Inc
	(m)	(cm/s)	(cm/s)	degrees
Leak	94.88 (Sea floor)	6.9±0.3	-1.4±0.2	76±2
	93.93	8.4±0.3	-1.8±0.3	76±2
	92.90	9.2±0.3	-2.0±0.3	75±2
	91.8	9.8±0.3	-2.2±0.3	74±2

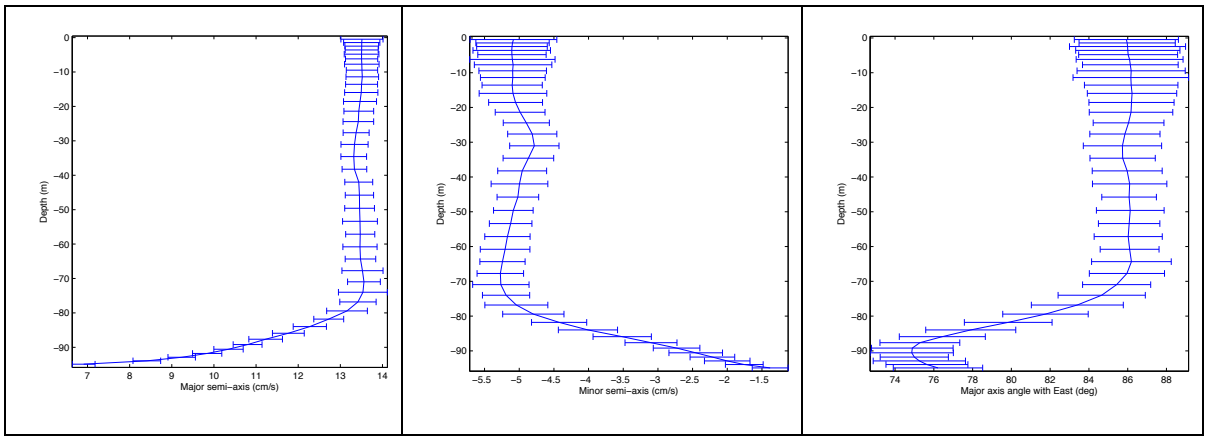

Figure 3: Profile of the M2 ellipse at the leak taken from BOM. From left to right; Major half-axis, minor half axis, and rotation of the ellipsis relative to east direction. Negative minor value indicates a clockwise rotation, with angle Inc, of the ellipse from east.

Doing a similar PCA analysis of the raw current time-series gives a different view, Figure 4. It is evident that the M2 ellipse is the main tidal component. However, the principle direction is different when performing PCA on the velocity vector. The tidal prediction gives a max current just above 0.2 m/s, with a mean tidal current below 0.1 m/s. The mean velocity profile is hence larger than the mean tidal signal. Since the period of integration includes storm passages, the BOM simulation also has periods of considerably higher velocities. The profile is shown in Figure 4 represent the max velocity at each depth, and is not an extracted profile.

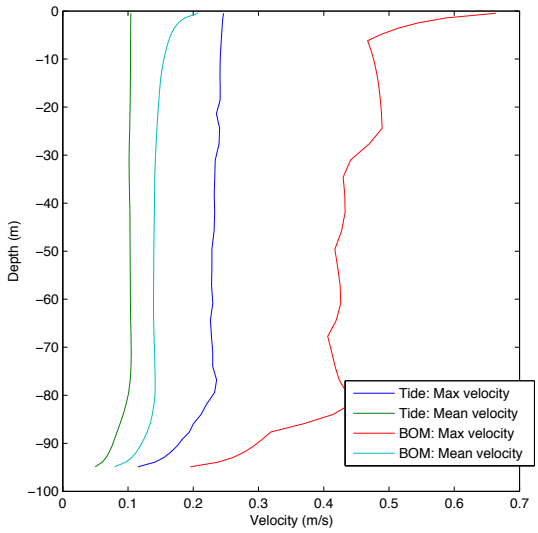

Figure 4: Mean and maximum velocity profiles from the tidal prediction and BOM.

An important factor for local mixing is the current shear along the sea floor. Figure 5 shows the time series for the velocity shear, du/dz, in the grid cell closest to the bottom. The mean value of this time series is 0.0178 and standard deviation 0.0086. A gliding mean can be created, however due to the resolution it is not expected that BOM can provide accurate shear at the bottom boundary layer.

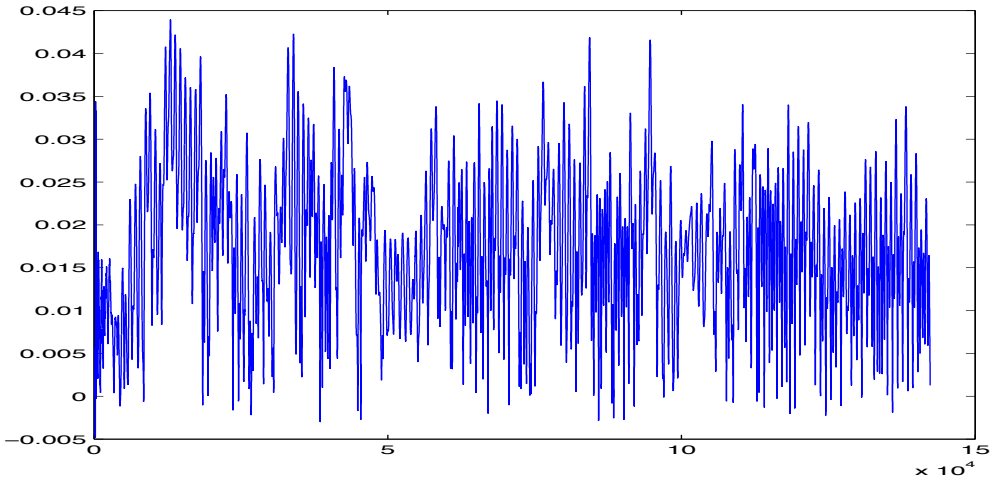

Figure 5: BOM results: Raw time series for du/dz at the seafloor, i.e. in the center of the first grid cell at the leak location.

Since the models are quite different it is considered that the study is easier accessible if each of the model results are reported in self-contained sections.

Executing the scenarios

The NIVA chemical model.

An interaction between the seawater and the sediments plays an important role in the biogeochemical cycling. The benthic fluxes of chemical elements affect directly the acidification characteristics (i.e. pH and carbonate saturation) and also determine the functionality of the benthic and pelagic ecosystems. In many regions redox state of the near bottom layer can oscillate in connection with supply of organic matter (OM), physical regime and coastal discharge influence.

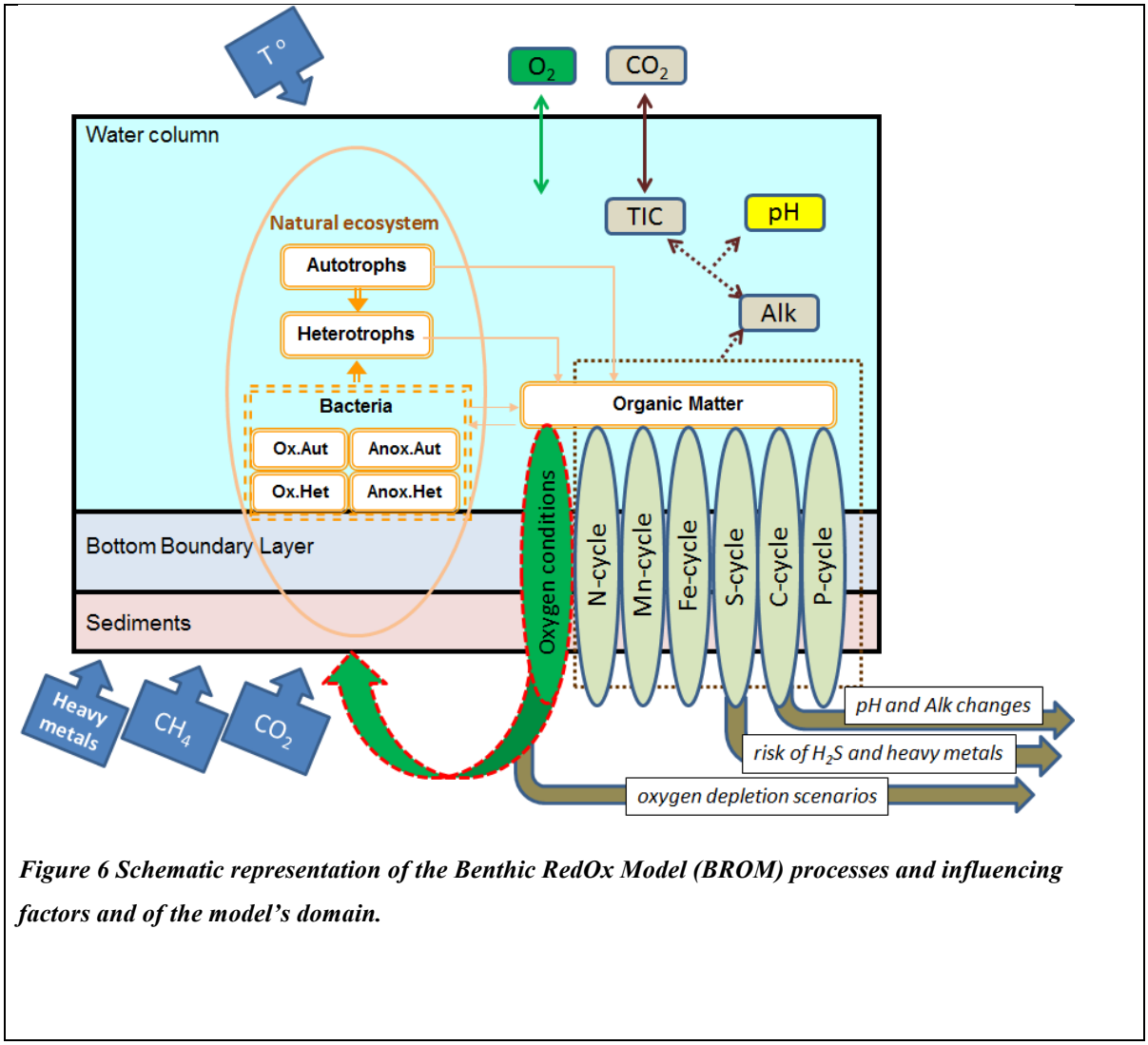

Figure 6 Schematic representation of the Benthic RedOx Model (BROM) processes and influencing factors and of the model's domain.

We use a 1-dimensional C-N-P-Si-O-S-Mn-Fe vertical transport-reaction Bottom RedOx Model (BROM) describing the sediments and bottom boundary layers (BBL) and the water column coupled with biogeochemical block simulating changeable redox conditions, and the carbonate system processes block (Yakushev, Protsenko, Bruggeman, 2014, in preparation). In BROM we parameterize OM formation and decay, reduction and oxidation of species of nitrogen, sulfur, manganese, iron, and the transformation of phosphorus, silicate and carbon species. BROM includes a simplified ecological model with phytoplankton, heterotrophic organisms, aerobic autotrophic and heterotrophic bacteria, anaerobic autotrophic and heterotrophic bacteria as it was described in (Yakushev et al., 2007). Carbonate system equilibration is modeled using standard approaches, the components of total alkalinity significant in suboxic and anoxic conditions (i.e. forms of S, N, redox reactions connected with N, Mn, Fe cycling) were taken into account. BROM is coupled to FAMB (Bruggeman, Bolding, 2014) as a transport model and a biogeochemical model. The model's domain includes the water column, the BBL and the upper layer of the sediments (Figure 6). To parameterize the water column turbulence we used results of simulation of turbulent mixing performed with GOTM (Bolding et al., 2001). In the limits of the BBL mixing was assumed to be constant. In the sediments molecular diffusion and bioirrigation/bioturbation were parameterized.

Preliminary simulations based on North Sea data available from observations and experiments (mainly for the water column, in particular from the ECO2 cruises) has been used as forcing data for the model' biogeochemistry.

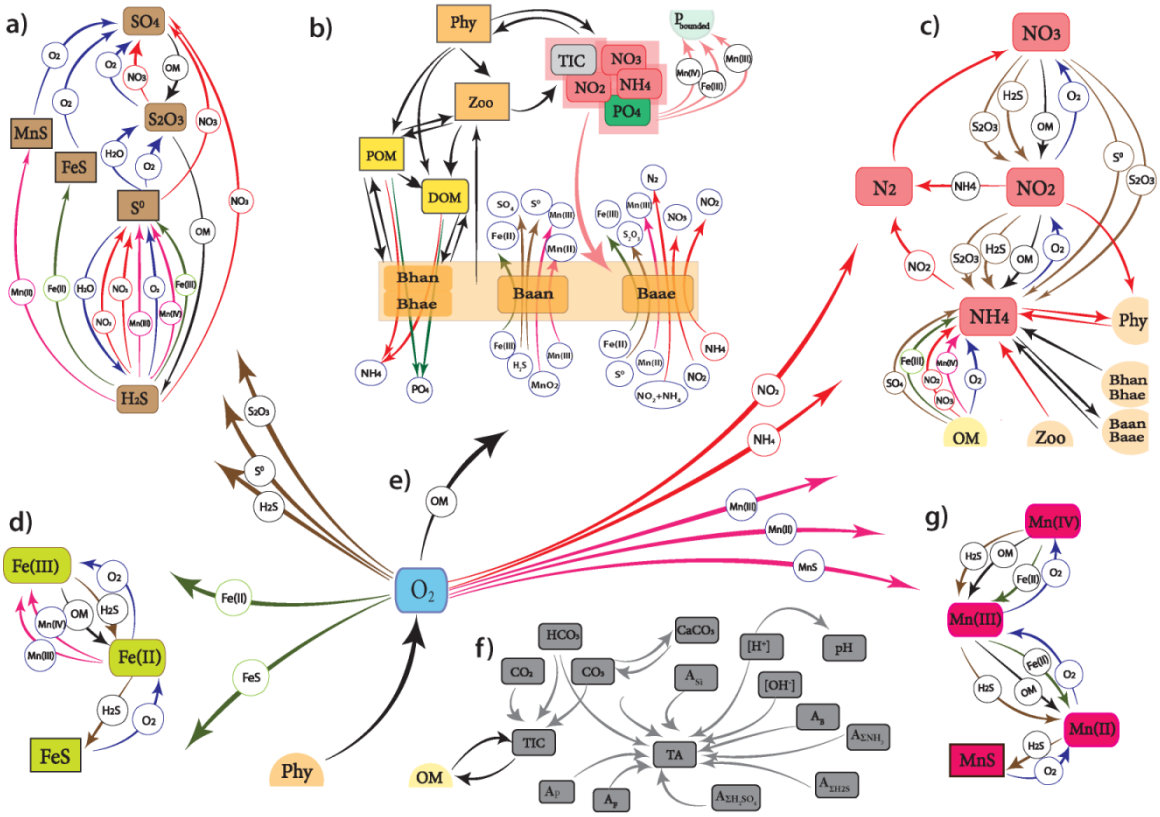

Figure 7 Flow-chart of biogeochemical processes represented in the Benthic RedOx Model (BROM). transformation of sulphur species (a), ecological block (b), transformation of nitrogen species (c), transformation of iron species (d), processes affecting dissolved oxygen (e), carbonate system and alkalinity (f), transformation of manganese species (g).

The aim of the baseline simulations with BROM was to model the **possible extreme natural changes** at the sediment-water interface with a decreased mixing in the BBL and an appearance of a periodic bottom anoxia. Such situations can release in the methane seepages (Figure 8) that can be places of a potential CO_2 release.

In addition to the model formulations described in the previous report the following was added:

Bioturbation/bioirrigation

Bioturbation activity (i.e. mixing of sediment particulates by burrowing infauna) and bio-irrigation (i.e. flushing of benthic sediment by burrowing fauna through burrow ventilation) were parameterized in the model. On the base of the mesocosm experiments with the North Sea sediments (ECO2 D4.1 Report, 2014) the biodiffusion coefficient was

found to be 2 - 5 cm^2yr^{-1} (0.06 – 0.16 10-10 m^2s^{-1}) and the maximum bioturbation depth was 0.5-2.2 cm, with higher values in natural conditions. Since in the model we should parameterize effect of both bioturbation and bioirrigation we assumed the constant Kz_bio= 10.10-10 m^2s^{-1} in the upper 2 cm with an exponential decrease deeper in the sediment. A dependence of Kz_bio on oxygen was introduced to parameterize the absence of bioturbation/bioirrigation in case of anoxia.

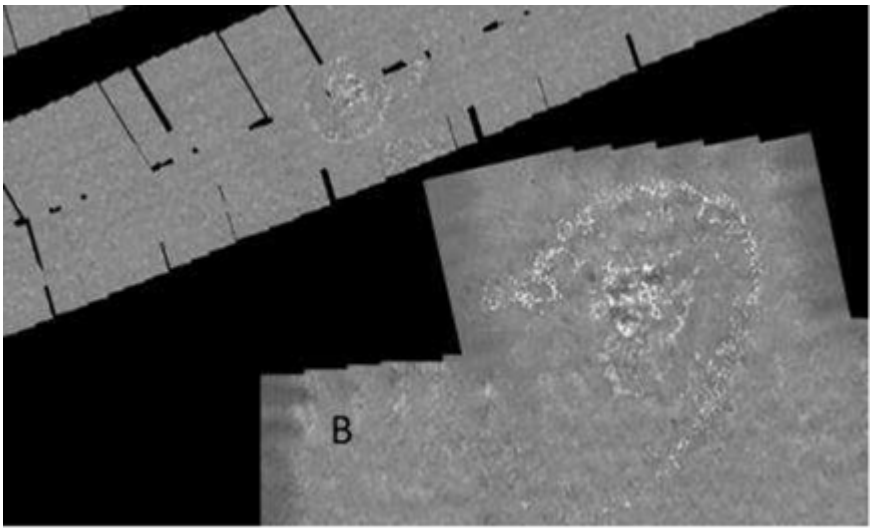

Figure 8: Photomosiaic of a seafloor seep site in the Central Norht Sea. Note the semicircular seabed structures where white bacterial mats mark the aereas with the most intense active seepage. Modified from (Graham et al., 2014)

Carbonate system

In this version of the model the reactions were divided in 2 groups kinetic processes and protolithic processes following the existing approaches (Boudreau, 1987, Luff et al., 2001, Jourabchi et al., 2005 and others). Protolitic reactions are fast compared to the time step and the equilibrium concentrations of the chemical element species can be calculated using mass action laws and equilibrium constants for the seawater (Millero, 1995). That allowed not to have a special state variable for example, for pH, but to calculate its value every time step. Than this pH value was used for calculations of the chemical equilibrium

constants needed to describe the related processes (i.e. carbonates precipitation/dissolution, carbonate system parameters concentrations etc.).

Total alkalinity, A_T, was s model state variable. Following the formal definition of A_T (Jorgensen et al., 1990, Dickson, 1981) the following alkalinity components were considered:

$$A_T=A_C+ A_B + A_P + A_{Si} +A_{NH} +A_{HS} +A_F + [OH^-].- [H^+] + A_{OM}$$

The carbonate alkalinity, A_C , the phosphoric alkalinity, A_P, the ammonia alkalinity, A_{NH}, and the hydrogen sulfide alkalinity, A_{HS}, were calculated from the corresponding model state variables according to (Luff et al., 2001, Volkov, 1984). The boric alkalinity, A_B, and the hydrofluoricalkalinity, A_F, and were calculated from salinity. Besides this the following redox reactions, that affect alkalinity through production or consumption of $[OH^-]_T$ or $[H^+]$ were considered in the model:

$4Mn^{2+} + O_2 + \mathbf{4H^+} \rightarrow 4Mn^{3+} + 2H_2O$

$4Mn^{3+} + O_2 + \mathbf{6OH^-} \rightarrow 4MnO_2+6H_2O$

$2MnO_2 + \mathbf{7H^+} + HS^- \rightarrow 2Mn^{3+} + 4H_2O+S^0$

$2Mn^{3+} + HS^- \rightarrow 2Mn^{2+} + S^0 + \mathbf{H^+}$

$Mn^{2+} + H_2S \rightarrow MnS + \mathbf{2H^+}$

$4Fe^{2+} + O_2 + 2H_2O \rightarrow 4Fe^{3+} + \mathbf{4OH^-}$

$Fe^{2+} + MnO_2+\mathbf{4H^+} \rightarrow Fe^{3+} +Mn^{2+} +2H_2O$

$2Fe^{3+}+HS^- \rightarrow 2Fe^{2+}+S^0+\mathbf{H^+}$

$Fe^{2+} + H_2S + HCO_3^- \rightarrow FeS + CO_2 + H_2O + \mathbf{H^+}$

$4S^0 + 3H_2O \rightarrow 2H_2S + S_2O_3^{2-}+ 2\mathbf{H^+}$

$2S^0 + O_2 + H_2O \rightarrow S_2O_3^{2-} + 2\mathbf{H^+}$

$4S^0 + 3NO_3^- + 7H_2O \rightarrow 4SO_4+ 3NH_4^+ + 2\mathbf{H^+}$

$S_2O_3^{2-} + 2O_2 + 2\mathbf{OH^-} \rightarrow 2SO_4^{2-} + H_2O$

$3H_2S + 4NO_3^- + 6\mathbf{OH^-} \rightarrow 3SO_4^{2-} + 2N_2 + 6H_2O$

$CaCO_3 \rightarrow Ca^{2+} + CO3^{2-}$

Results

The model simulates the basic features of the ecosystem development and shows a possibility of periodic replacement of oxic conditions with anoxic, that leads to changes in the distributions of the parameters and their fluxes. The seasonality in production and destruction of OM together with the mixing seasonality lead to a vertical displacement of the oxic/anoxic interface from the sediments in winter to the water in summer. This affects distribution of sulfur species, nutrients (N and P), redox metals (Mn and Fe) and carbonate system parameters. Bacteria play a significant role in the fate of OM due to chemosynthesis (autotrophs) and consumption of DOM (heterotrophs).

Carbonate system

The results of the baseline simulations of the carbonate system parameters are shown in Figure 9 and Figure 10.

The natural seasonal changes of the carbonate system parameters are the following. In the limits of the BBL:

- pH oscilated from 7.6-7.7 in oxygenated period to 7.2 in winter.
- pCO_2 changed from 800-1200 in oxygenated period to 2500 ppm in anoxic period
- The bottom water is oversaturated regarding calcite and close to the saturation regarding aragonite in oxygenated period to undersaturated in anoxic period

During the oxygenated period the sediment is oversaturated in regards of calcite and precipitation of $CaCO_3$ occurs, while during the anoxic period this $CaCO_3$ degrades.

In the upper 12 cm of the sediment pH is about 7.1, pCO_2 is about 7300 ppm. The modeled pH maximum in the upper mms of the sediment in the period before the bloom is connected with chemosynthesis maximum that leads to an intensive CO_2 consumption.

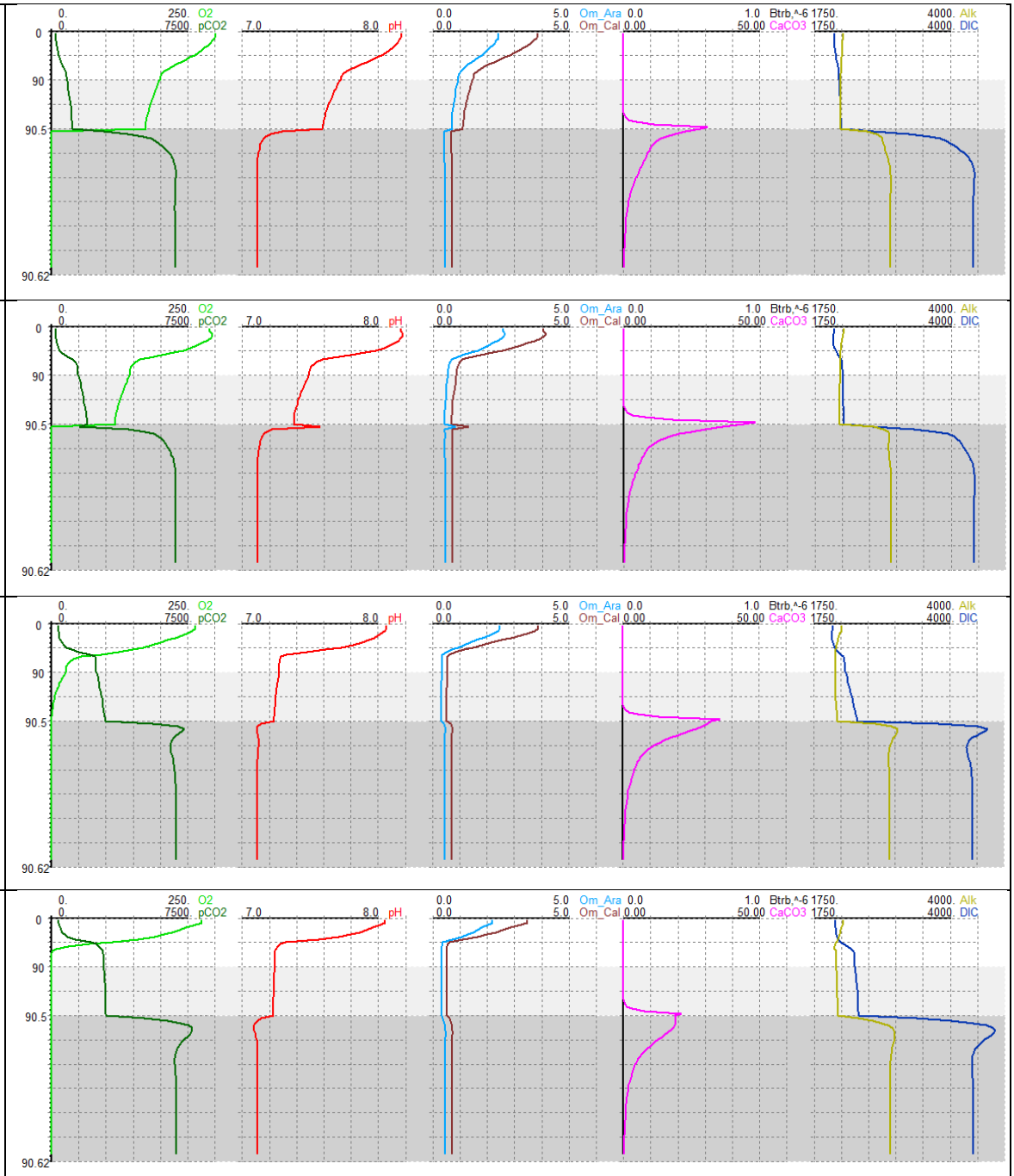

Figure 9: Vertical distributions of the modelled chemical parameters in the winter well-mixed conditions (day 90), in the period before the bloom (day 140), in the period of organic matter production and formation of pycnocline (day 215) in the period of stagnation and bottom anoxia (day 300).

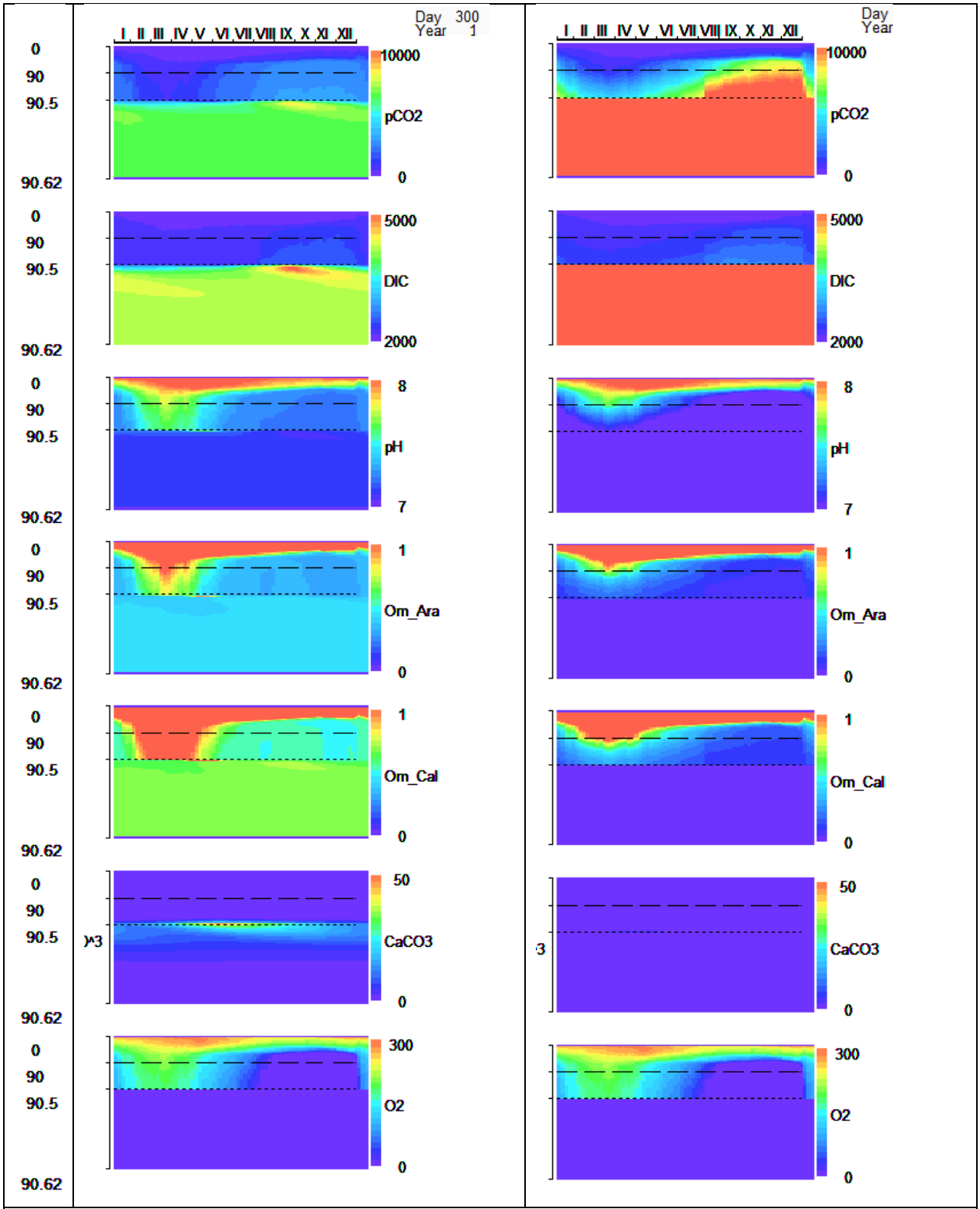

Figure 10 Simulated seasonal variability of the modelled chemical parameters: baseline simulation (left) CO_2 leakage Scenario Chimney reactivation (~150T/d, 500m diameter circle), after 70 years (right)

The main results from this run is that the undisturbed natural conditions can be variable, with significant season variations in the BBL of Omega values (from 0.3 to 1.2 for calcite and from 0.2 to 1.0 aragonite), and pH changes from 7.2 to 7.7. Nevertheless there exist conditions for the $CaCO_3$ precipitation and storage through all the year.
The baseline simulations discussed reproduced the same seasonal variability for several tens of years, and they were used as an initial condition for the leakage scenarios run.

CO_2 leakage simulations

The goal of this numerical experiment was an assessing of the strength of environmental perturbations caused by the CO_2 scape from marine CCS (Blackford et al., 2009) using the scenarios recommended.
We analyzed the Scenario 1 Chimney reactivation (~150T/d, 500m diameter circle), releasing 4341 mmolC $m^{-2}d^{-1}$. It was parameterized an addition of CO_2 to the low boundary of the model (12 cm in the sediment). It was assumed that this CO_2 dissolves in the water since the concentrations reached the equilibrium with the gas phase (taken, according to (ECO2 D4.1 Report, 2014) data as 1700 molC m^{-3}). The vertical transport of this signal upward was the molecular diffusion in, than this transport could be accelerated due to bioturbation in the upper 2 cm sediments layer. This transport seems to be a very rude approximation, since a potential formation of a CO_2 bubble inside the sediment can destroy the sediment.
The results of this experiment (Figure 10) is that after 70 years:

- calcite and aragonite saturation state never exceeds 1 at the bottom,
- $CaCO_3$ doesn't forms,
- pH in the bottom water drops down to less than 7.1.
- pH decrease leads to the dissolution of sulfides of Mn and Fe, and release of sulfide with a positive feedback to anoxia development. Such changes in the biogeochemistry should cause the drastic consequences in the benthic ecosystem.

Future plans

The results presented are of preliminary character. The baseline simulations were made to reproduce the possible extreme natural changes, and were not validated using the

observations and experimental data of the sediment composition. At this stage there had not modeled any influence of lowering pH at the physiology of organisms and bacteria. We plan to:

- Use data collected in the area (from WP4) to validate the model first of all in the vicinity of the low boundary.
- Parameterize some more important processes (i.e. dependence of the bioturbation on the CO_2, Si sysle)
- Calculate the fluxes of the carbonate system parameters in the natural conditions and during the leaks experiments.
- Parameterize enchanced vertical transport of CO_2 in case of the reaching of the saturation in the lower boundary.
- Produce baseline simulations for the permanently oxic sediments typical for the Sleipner area.
- Estimate time after which the CO_2 leak can be detected using the measurements in the bottom water (i.e. pH).

The Geomar model

The Footprint of a CO_2 Leaking Well in the Water Column

Background:

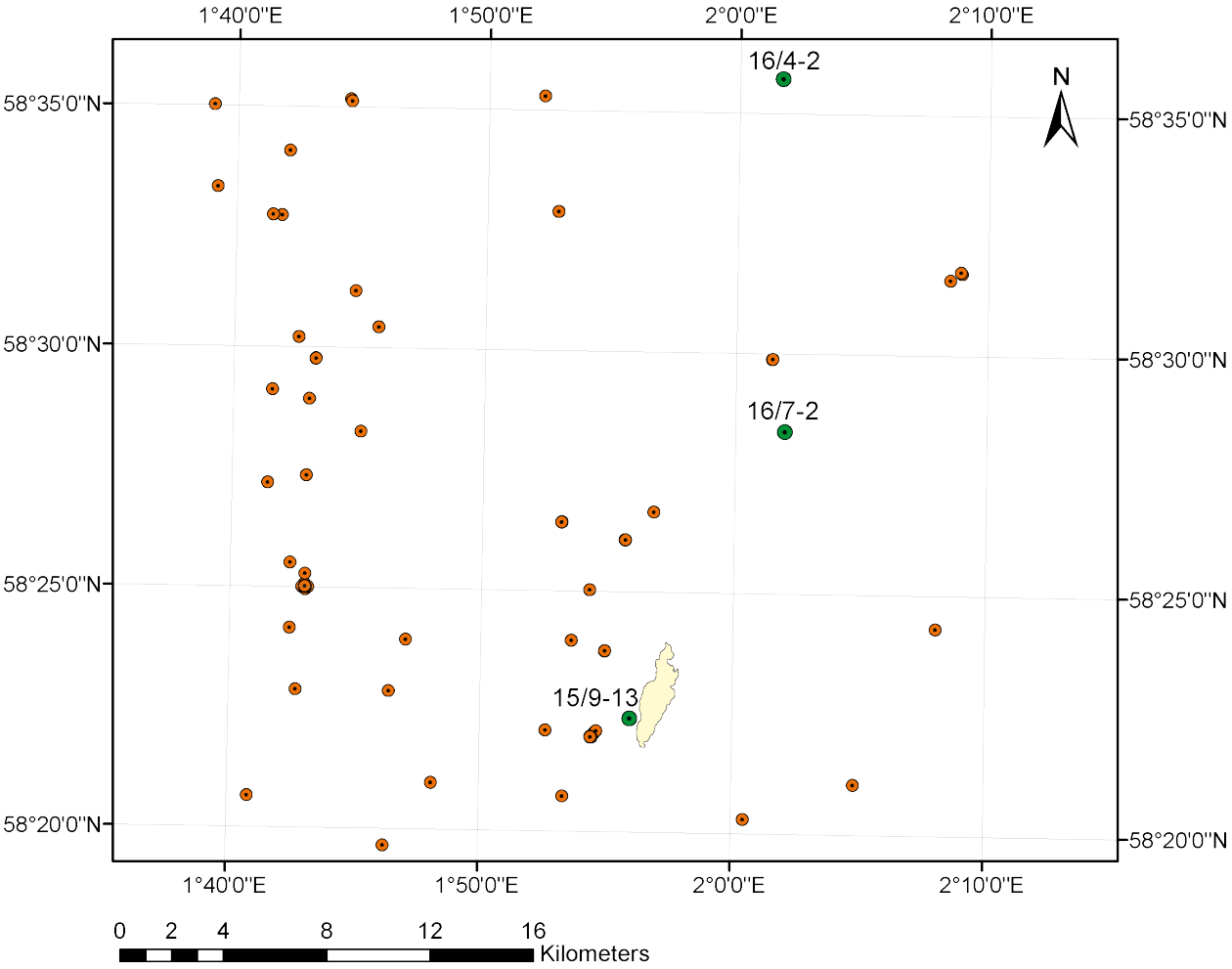

Figure 11: *Map of the Sleipner area showing the location of three investigated abandoned wells (green dots), which are leaking methane into the water-column, the location of other wells in that area (orange dots), and the extent of the subsurface CO_2 plume in 2008 (yellow).*

Wells that penetrate CO_2 storage locations represent potential conduits for focused upward migration of gas that might allow CO_2 to leak into the water-column. Considering the high number of wells that have been drilled in the North Sea (i.e. more than 15 000) the leaky well scenario is possibly the most likely. In order to estimate potential leakage rates and

bubble sizes Geomar investigated three abandoned wells at 81-93 m water depth in the Norwegian sector of the North Sea, all of which show gas seepage into the bottom water (**Figure 11**). The seep gas at the wells consists mainly of methane (85-89 Vol.%) that originates from shallow gas pockets in the sedimentary overburden above the gas reservoirs that the wells were drilled into. This is in agreement with high amplitude anomalies in the seismic data (i.e. bright spots and zones with chaotic signatures) indicating the evidence of gas in 600-750 m below the seafloor. The isotopic signature of the emanated gas, i.e. C1/C2+ ratio larger than 1000, and δ13C values of CH4 lighter than-70 ‰ VPDB clearly points towards a biogenic origin.

Direct gas flow measurements result in a total seabed gas flow between 1 and 18.5 tons of CH4 per year per well. A combined bubble size distribution was determined from video-analysis of seeping gas bubbles, combining 274 bubble size measurements at well 16/4-2 and well 15/9-13 (**Figure 13**A). It is suggested to be representative for bubbles released from the fine to medium grained clayey sand found at the investigated wells.
Considering that leakage properties are mainly controlled by the geology, rather than by the gas species, potential CO_2 leakage rates and bubble sizes might be similar to the ones observed at the methane leaking wells. In order to access the impact of a CO_2 leaking well we estimate the footprint of the dissolved CO_2 and the corresponding pH drop in the water column by numerical modeling. The scenario is based on a leakage rate of 20 t CO_2 yr^{-1} and the combined bubble size distribution found at the investigated wells.

CO_2 Bubble Dissolution

In order to simulate the shrinking of a CO_2 bubble due to dissolution in the water column, and its expansion due to decreasing pressure in the course of its ascent and gas stripping a numerical bubble dissolution model (BM) was used. The model solves a set of ordinary differential equations describing these processes for each of the involved gas species (CO_2, N_2, and O_2) using the built-in NDSolve object of Mathematica. Thermodynamic and transport properties of the gas components, such as molar volume, gas compressibility, and gas solubility in seawater, were calculated from respective equations of state (Duan et al., 1992; Duan, 2006; Geng and Duan, 2010; Mao and Duan, 2006), and empirical equations

for diffusion coefficients (Boudreau, 1997), mass transfer coefficients (Zheng and Yapa, 2002), and bubble rise velocities (Wüest et al., 1992) taking into account local pressure, temperature and salinity conditions in the Sleipner area as measured by CTD casts. The leakage depth was set to 80 m below the sea-surface.

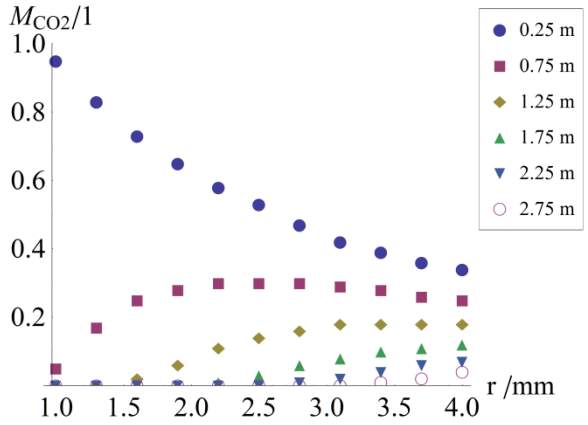

Figure 12: Model results showing the mass of CO_2 dissolution normalized to the initial CO_2 bubble content (M_{CO2}) versus bubble radius (r) at a certain depths above seafloor (legend).

Simulation results indicate that the rate of CO_2 dissolution strongly depends on the initial bubble size (Figure 12). Small bubbles tend to dissolve closer to the seabed due to a reduced lifetime and a slower bubble rise velocity compared to larger ones. While a bubble of 1 mm radius loses 95% of its initial mass within the first 0.5 m of its ascent, a 4 mm bubble is able to transport 66% into shallower depth (i.e. > 0.5 masf). Thus, small bubbles clearly increase the acidification impact on the marine benthos at a given leakage rate. Based on the bubble size distribution found at methane leaking abandoned wells ~ 50 % of the initially released CO_2 dissolves within the lower 0.5 m of the bottom water (**Figure 13**B). Simulations further suggest that the dissolution behavior of the size spectrum can be perfectly represented by bubbles with a unique radius of 2.7 mm (**Figure 13**B). Bubbles of the spectrum will be depleted in CO_2 within the lower 3 m of the water column (**Figure 13**B). Hence, the impact of a CO_2 leaking well is clearly limited to bottom waters.

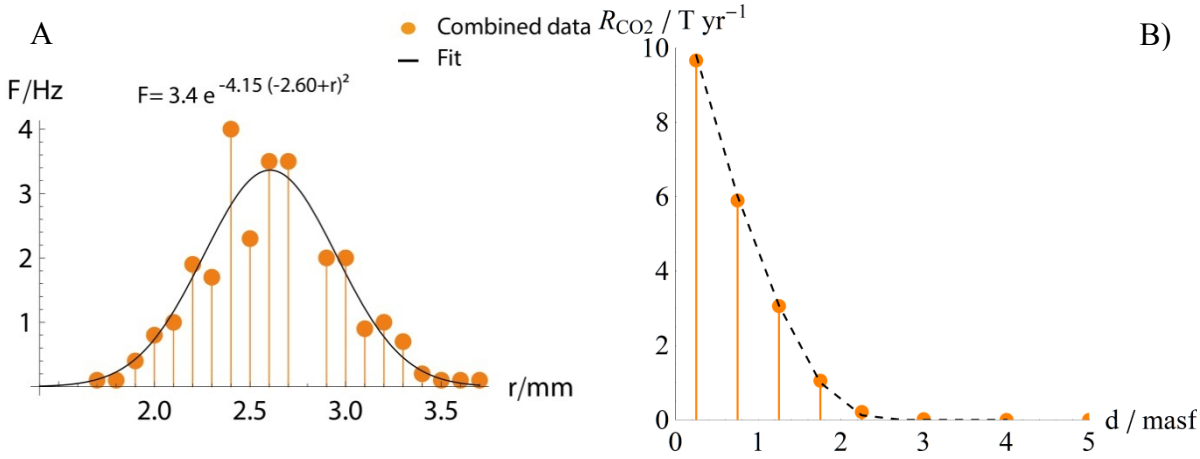

Figure 13: ***A)*** *Measured bubble release frequency (F) versus bubble radius (r), and Gaussian fit for the combined bubble size distribution based on measurements at wells 15/9-13 and 16/4-2. The error, s^2, of the fit is 0.18.* ***B)*** *Model results based on the combined bubble size spectrum (orange dots) showing the rate of CO_2 dissolution (R_{CO2}) as a function of depth above the seafloor (d). The dissolution behavior of the bubble size spectrum can be perfectly represented by bubbles of a unique radius of 2.7 mm (dashed line).*

Plume Dispersion on a Small Scale

In order to simulate the spread of dissolved CO_2 in the water column a small scale plume dispersion model (PM) of 100*25*10 m was used. The model solves a set of partial differential equations describing the turbulent flow and the resulting transport of CO_2 in 3D using build-in physical modules and time-dependent solvers of COMSOL Multiphysics. Transport properties taking into account local current velocities as measured by ADCP deployments in the Sleipner area in August 2012 (**Figure 14**A). As a result of lacking ADCP data in the lower 3.7 m of the water column a logarithmic decrease of the velocity towards the bed was included taking into account friction at the bed (**Figure 14**B). The spatial resolution of the PM varied between 0.075 and 1.75 m. In total 4 leaky well case studies were run distinguishing between different driving factors, such as current velocities (i.e. low, high, and slack water) and leakage type (i.e. diffusive vs. focused) (Table 3). This allows the identification of lower and upper thresholds defining the impact of CO_2 leakage in the water column. Here the environmental impact is stated as the spatial

footprint of the dissolved CO_2 plume at the seafloor (i.e. partial pressure of CO_2 above 490 µatm, corresponding to a pH drop of -0.09 units exceeding the natural variability of CO_2 in North Sea bottom waters).

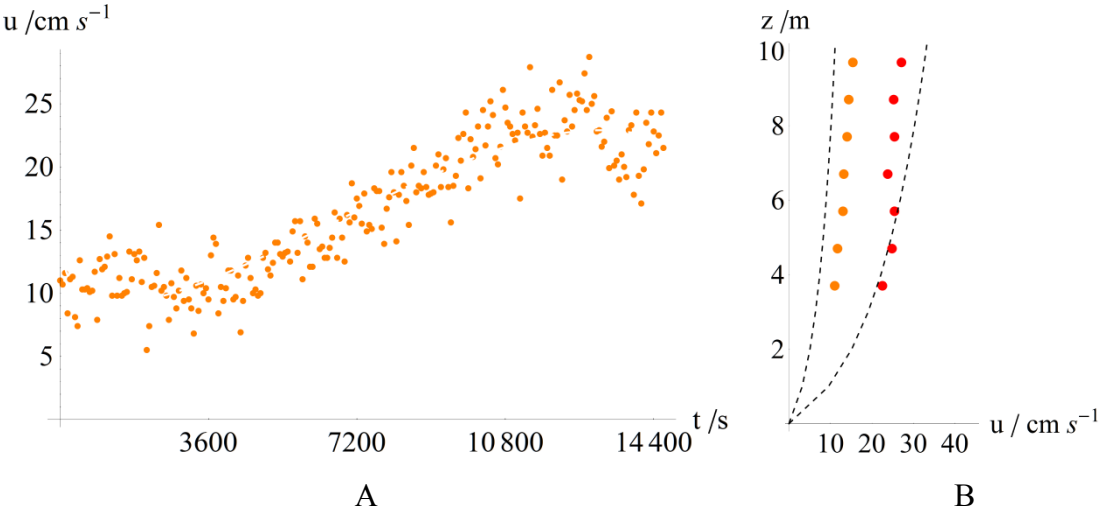

Figure 14: ***A)*** *Measured current velocity (u) versus time (t) at 3.7 masf.* ***B)*** *Depth above the seafloor (z) versus measured current velocity (u) at t=0(orange dots) and t=12060 s (red dots), and fit that is used in the numerical model (dashed line). Data indicate a logarithmic decrease of the velocity towards the bed. However, uncertainty remains in the lower 3.7 m of the water-column due to a lack of data– this is where CO_2 bubbles dissolve.*

Simulation results indicate that the impact of a CO_2 leaking well is clearly limited to bottom waters and a small area around the leak (Figure 15 and Table 3). Particularly at strong current velocities the leak will be hardly detectable considering the slight increase in pCO_2 of ~330 µatm, the tiny drop in pH of 0.25 units, and the small extent of the solid CO_2 plume, i.e. less than 30 m^2 (Table 3, Scenario 2).

Despite the focused leakage scenario at low current velocities and at slack water the resulting elevation in pCO_2 is found to be comparable to the natural variability of CO_2 (i.e. DIC of 2175 µmol kg^{-1} in summer, Bozec et al. 2006). Therefor the impact of both focused CO_2 leakage at strong currents and diffusive CO_2 leakage is considered to be negligible (Table 3**,** Scenario 1 and 2). By contrast, at weak currents the focused leakage of CO_2 results in elevated pCO_2 values of up-to 1665 µatm and an area of ~ 80 m^2 is exposed

to pCO_2 values that exceed the threshold of natural CO_2 variability.
Slack water bears the highest risk for the marine benthos because the dilution and mixing of low pH waters with ambient seawater is inhibited. However, the substantial drop in pH of more than -1.6 units appears to occur only in the direct vicinity of the leak and tends to last for a short time (tens of minutes).

We conclude that even though CO_2 leakage from the storage formation is possibly most likely to happen along an existing well, the environmental impact is expected to be rather small to negligible making the detectability of such a leak highly challenging. Strong currents and tidal cycles, both prominent in the North Sea efficiently diminish the spread of low pH waters into the far field of a leak.

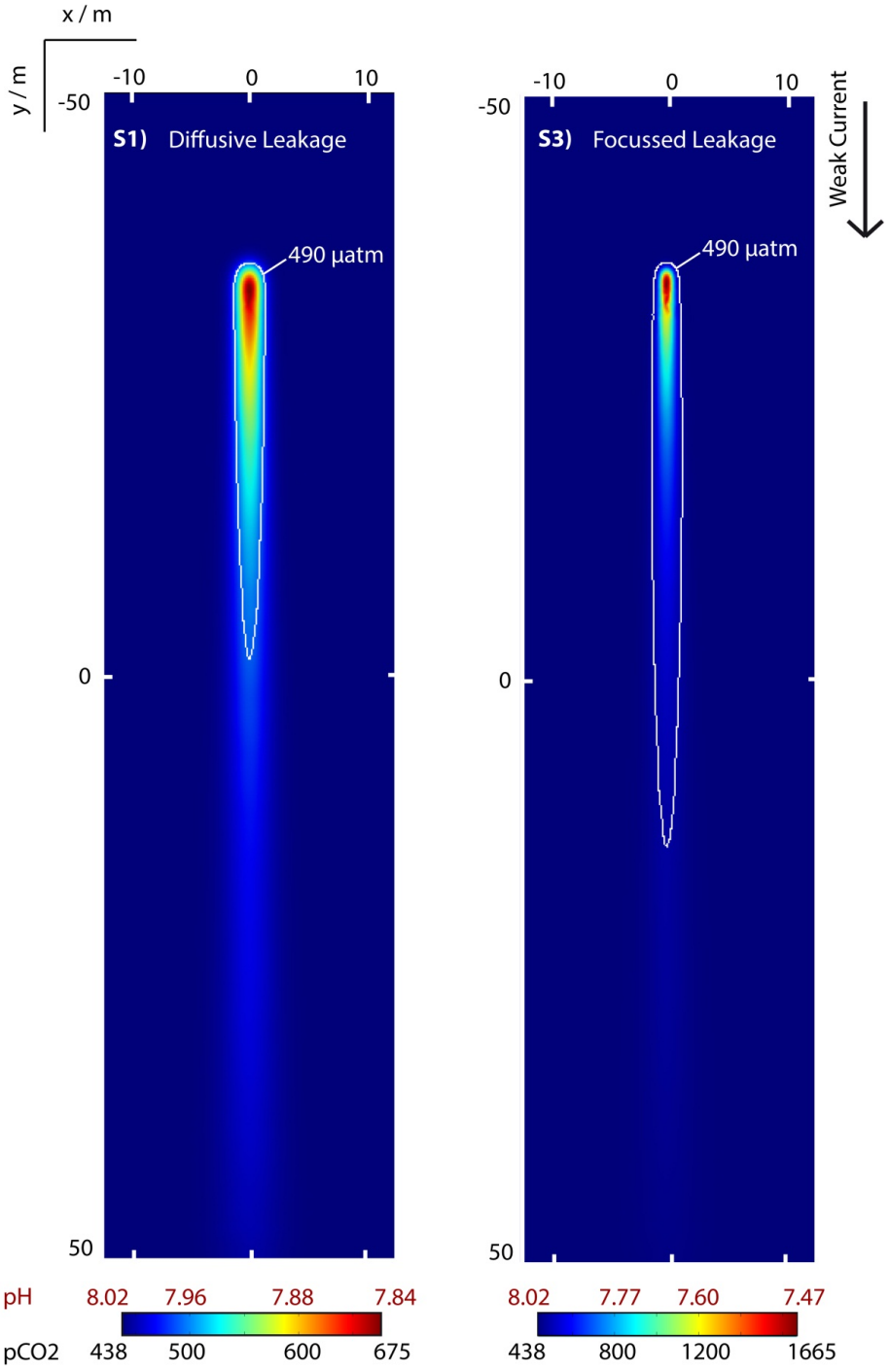

Figure 15: Top-view on the CO_2 footprint at the seafloor in m² for diffusive (S1) and focused (S3) leakage based on an annual CO_2 leakage rate of 20 tons, and weak current velocities. The contour line represents the threshold of natural CO_2 variability of 490 µatm corresponding to a pH-drop of -0.09 units.

Table 3: Summary of model parameters used in the four leaky well case studies and resulting environmental impact.

Parameter	**Scenario 1 Diffusive**	**Scenario 2 Focused**	**Scenario 3 Focused**	**Scenario 4 Focused**
Leakage Rate / t CO_2 yr^{-1}	20	20	20	20
Leakage Area / m^2	10	1	1	1
Current velocity	Weak[1]	Strong[2]	Weak[1]	Slack[3]
Background pCO_2 /µatm	438	438	438	438
Background pH / units	8.02	8.02	8.02	8.02
Environmental Impact				
Max pCO_2 / µatm	675	765	1665	21496
Max pH drop / units	-0.18	-0.25	-0.55	-1.64
CO_2 Footprint* / m^2	57	28	78	11

* at the seafloor with pCO_2 values above the threshold of natural variability of 490 µatm corresponding to a pH drop of more than -0.09 units

[1]Weak: V_c=0.065*Log(1+z)

[S]2trong:V_C=0.138*Log(z+1)

[3]Slack: Very weak current of V_C=0.005 m s^{-1} duration of 10 min

The HWU model

Bubble/droplet plume formation

The HWU model is designed to show the bubble/droplet plume formation, dynamics and dissolution. In addition to this, the model shows, on the small scale, the distribution of the dissolved CO_2 being ejected into the water column from the dissolving bubble plume.

Governing equations for CO_2 and seawater plumes

The CO_2 bubble plume is referred to as the dispersed phase (subscript *d*), and the seawater carrier phase (subscript *c*), with the void fraction α calculated as:

$$\alpha_c + \alpha_d = 1$$

large eddy simulation based governing equations for the seawater carrier phase are defined as:

$$\frac{\partial \bar{\rho}}{\partial t} + \frac{\partial \bar{\rho} u_i}{\partial x_i} = \dot{w}_{co_2} \tag{1}$$

$$\frac{\partial \bar{\rho} u_i}{\partial t} + \frac{\partial \bar{\rho} u_i u_j}{x_j} = -\frac{\partial \hat{p}}{\partial y} + \frac{\partial D_{ij}}{\partial x_i} + (\bar{\rho} - \rho_0) g + \dot{F} \tag{2}$$

$$\frac{\partial \bar{\rho} \hat{\phi}_k}{\partial t} + \frac{\partial \bar{\rho} \hat{\phi}_k u_j}{\partial x_j} = \frac{\partial}{\partial x_j}(\bar{\rho} D_k \frac{\partial \hat{\phi}_k}{\partial x_j}) + \frac{\partial \bar{\rho} \hat{q}_k}{\partial x_j} + \dot{w}_{co_2} \tag{3}$$

and the governing equations for the dispersed bubbles phase as:

$$\frac{\partial \hat{n}_d}{\partial t} + \frac{\partial \hat{n}_d u_{di}}{\partial x_i} = \hat{q}_{dn} \tag{4}$$

$$\frac{\partial \hat{\alpha}}{\partial t} + \frac{\partial \hat{\alpha} u_{dj}}{\partial x_j} = \hat{q}_{dco_2} - \frac{\dot{w}_{co_2}}{\rho_d} \tag{5}$$

$$\frac{\partial \bar{\rho}_d u_{dj}}{\partial t} + \frac{\partial \bar{\rho}_d u_{di} u_{dj}}{\partial x_j} = \hat{\alpha}(\bar{\rho}_d - \rho_w) g - \dot{F} \tag{6}$$

where $\bar{\rho}$ is the bulk density, (kg/m^3), u is the velocity (m/s), t is the time (s), x is the dimension (m), $\dot{w}$ is the mass exchange rate (kg/m^3·s), p as the hydrostatic pressure (Pa),

D is the dissipation term (kg/m·s^2), ρ_0 in the initial density of seawater (kg/m^3), g is gravity (m/s^2), $\dot{F}$ is the momentum exchange rate (kg/m^2·s^2), $\hat{\phi}$ is a scalar (temperature, salinity or CO_2 concentration), D_k is effective diffusivity (m^2/s), and $\hat{n}$ is the number density of bubble/droplet (m^{-3}), with a source term $\hat{q}$. The subscripts 'd', '*w*', 'CO_2' represent the dispersed phase, seawater and CO_2 respectively, with directional vectors represented though the subscripts '*i*', '*j*', '*k*'.

Mass and momentum exchange between two plumes

In order to solve the governing equations, sub-models for the mass and momentum exchange terms are required:

$$\dot{w}_{co_2} = (6\hat{\alpha})^{1/3}(\pi\hat{n})^{2/3} Sh\, D_f (C - C_0) \tag{7}$$

$$\dot{F} = 0.75\left(\frac{\pi}{6.0}\right)^{1/3} \rho_d \hat{\alpha}^{2/3} \hat{n}^{1/3} C_d \left|u_j - u_{dj}\right|\left(u_j - u_{dj}\right) \tag{8}$$

Eq. (7) is the mass exchange rate from CO_2 dissolution, where Sh is Sherwood number, C is the bubble surface CO_2 concentration (kg/m^3) and C_0 is the seawater CO_2 concentration (kg/m^3). Eq. (8) is the momentum exchange rate through the drag force between the bubbles and the seawater, where C_d is the drag coefficient. Modelling of the exchange rates of two plumes is described in the following sections.

Bubble/droplet plume formation

The bubble plume formation requires a selection of data, the leakage rates are as provided by WP1 and WP2, along with the extra 2 case studies as decided upon by CCT2. The leakage area has been provided allowing the prediction of a leakage flux. In addition, the prediction of bubble/droplet plume formation also requires the initial diameter (described by equivalent diameter, d_{eq} m), of the bubbles/droplets leaked from sediments. This can be estimated through the theories of gas bubble instability, the force balance where the CO_2 will remain attached to the sediment until buoyancy and drag forces exceed the tension between the bubble/droplet and the sediment surface as

$$\left[\left(\rho_w - \rho_{CO_2}\right)g\frac{d_{i,eq}{}^3}{6}\right]^2 + \left[\frac{C_d}{8}\rho_w u^2 d_{i,eq}{}^2\right]^2 = \left[d_{ch}\left(\sigma_{sw} + \sigma_{sed}\right)\right]^2 \quad (9)$$

where, ρ_w and ρ_{CO_2} are the density of seawater and CO_2 (kg/m^3), σ_{sw} is the surface/interfacial tensions of the CO_2 to seawater (N/m), and σ_{sed} is the surface/interfacial tensions of the CO_2 to the sediments (N/m). Further details may be found in the technical report on verified and validated application of droplet/bubble plume-, geochemical- and general flow- models or Dewar et al. (2013).

Bubble/droplet dissolution

The prediction of the rate of bubble dissolution is based upon the correlation proposed by Zheng and Yapa (2002) for bubbles in water in terms of the Sherwood number (*Sh*), defined by effective dissolution coefficient k_e, and diffusivity D_f, by:

$$Sh = \frac{k_e d_{eq}}{D_f} = f_k\left(d_{\text{eq}}, u_{\text{rd}}\right)\cdot\frac{d_{eq}}{D_f{}^{1-n}} \quad (10)$$

with an index of n = 0.5 for the diffusivity, d_{eq} (m) as the equivalent diameter and u_d (m/s) as the relative bubble velocity (m/s); the function f_k varies dependent on the bubble diameter:

$$f_k(d_{eq}, u_d) = \begin{cases} 11.3\left(\dfrac{u_d}{0.45 + 20 d_{eq}}\right)^{0.5} & d_{eq} < 5mm \\ 6.5 & 5mm < d_{eq} < 13mm \\ \dfrac{0.219462}{d_{eq}{}^{0.25}} & d_{eq} > 13mm \end{cases}$$

For droplets with hydrate film, as generally found in deep ocean scenarios, the estimation of Sherwood number is based on the Ranz-Marshall correlation with a deformation factor (Chen et al., 2003)

$$sh = \left(2 + 0.69\,\text{Re}^{1/2}\,Sc^{1/2}\right)\left(\frac{A_{eff}}{A_{eq}}\right) \quad (11)$$

with the deformation factor as:

$$\left(\frac{A_{eff}}{A_{eq}}\right)=\left(1+4.67075\times10^{-4}\,\mathrm{Re}-1.1871\times10^{-6}\,\mathrm{Re}^2+1.4766\times10^{-9}\,\mathrm{Re}^3\right)$$

Bubble/droplet momentum interactions with seawater

The momentum exchanges of bubbles with seawater are governed by the buoyancy and drag forces, for which the drag coefficient must be modelled for bubbles and droplets with/without deformation. A correlation of drag coefficient is developed from a number of lab/field experiment studies, which may be found in the technical report on verified and validated application of droplet/bubble plume-, geochemical- and general flow- models or in Dewar et al. (2013). A best-fit model to the data at $\mathrm{Re}<400$ for bubbles and $\mathrm{Re}<800$ for droplets is

$$C_d=\frac{24}{\mathrm{Re}}f(\mathrm{Re}) \qquad (12)$$

Correlations for the friction factor $f(\mathrm{Re})$, as a function of Reynolds number, Re, are developed through curve fitting for the droplets and bubbles and formulated using constants data given:

$$f(\mathrm{Re})=1+0.045\,\mathrm{Re}-A\,\mathrm{Re}^2+B\,\mathrm{Re}^3$$

	A	B
Droplet without Hydrate:	1.50×10^{-4}	1.60×10^{-7}
Droplet with Hydrate:	7.50×10^{-5}	8.00×10^{-8}
Bubble without Hydrate:	1.50×10^{-4}	3.20×10^{-7}
Bubble with Hydrate:	1.20×10^{-4}	3.20×10^{-7}

For $\mathrm{Re}>400$ for bubbles and $\mathrm{Re}>800$ for droplets the correlation proposed by Bozzano and Dent (2001) is employed:

$$C_d=f\left(\frac{a}{R_0}\right)^2 \qquad (13)$$

where the friction factor f is found to be:

$$f = \frac{48}{\mathrm{Re}}\left(\frac{1+12M^{1/3}}{1+36M^{1/3}}\right)+0.9\frac{Eo^{3/2}}{1.4\left(1+30M^{1/6}\right)+Eo^{3/2}}$$

and the deformation factor $(a/R_0)^2$ is found to be:

$$\left(\frac{a}{R_0}\right)^2 = \frac{10\left(1+1.3M^{1/6}\right)+3.1Eo}{10\left(1+1.3M^{1/6}\right)+Eo}$$

Environmental conditions and special considerations

Environmental conditions

The seawater and CO_2 properties are defined through the pressure controlled by the depth of the seawater, salinity and temperature profiles. The topography has been neglected in this small-scale two-phase model as the effects from the topography in the scale less than 1 km is negligibly small on the development of bubble and pH (and DIC) plumes. The depth has been taken from the BOM model, of 94.88 m. A range of ocean currents have been selected for the simulations, initially with no current, then analysing the currents mentioned earlier in this report using the data from the BOM model for both the major and minor velocity profiles.

Special considerations and assumptions

Data for the top sediment data to predict the initial bubble size (Eq. 9) have been taken from Ardmucknish bay, which although is on the other side of Scotland than the North Sea, is considered to have similar sediment properties to that of the North Sea.

For the leakage area, in all case studies, the leakage is spread across multiple grids, with the initial bubble sizes varied from 6.4 mm to 1.5 mm depending on the channel size of the sediments. Each grid size is uniform at 4m x 4m x 0.975m for the chimney reactivation and the bubbles are leaked from one pockmark location at any one moment, 50m x 50m x 0.975m for the elongated conduit, 4m x 4m x 0.975m for the blowout, and 0.8m x 0.8m x 0.975m for the leaky well, where for these three scenarios, the bubbles are leaked from multiple pockmarks, with the initial diameters (1.5mm – 6.5mm) varying with distance and

time. Each scenario is contained within 181 x 200 x 100 grid locations in the X, Z and depth (Y) directions respectively.

A fracture in the elongated conduit is unlikely to be 200m wide all the way across, although the fracture is likely to be within a 2000 x 200 m area. Therefore existing fractures and dimensions were looked at and linked with the grid of our small scale model to a width of between 50 and 200m varying based on the shape of a generic fracture. If the simulation was retained as a uniform 2000 x 200 m leak, it would not accurately show the bubble plume due to the low flux.

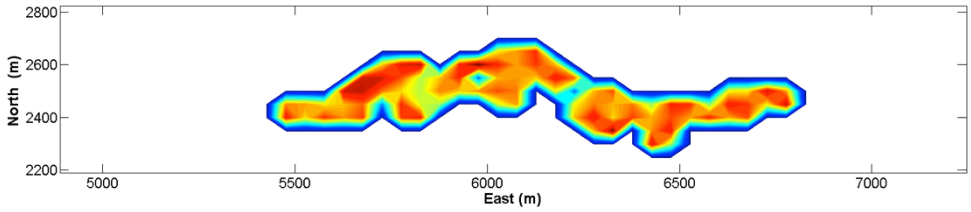

Figure 16: Generic fracture structure used for the elongated conduit scenarios (the bubble size in colour is used here to indicates the fracture structure)

Data for the seasonal variations has been previously shown (Dewar et al., 2013) to have little difference on the environment at this depth as there is only about 1.0 degree of change in temperature providing less than 1.0% variation in the overall plumes dynamics (pH, bubble dissolution). Therefore it was considered to be more worthwhile to utilise the computer resources to simulate the effects of the water current as this has been also shown to have one of the greatest effect on the dissolved CO_2 concentration.

Results from the HWU model

The following results provided by the simulations show the bubble plumes, which are presented by the bubble equivalent diameter (d_{eq}), number density of bubbles, plume height, along with spatial distribution of the bubble plume. The footprint on the seabed is then showed in terms of DIC and pH changes, showing the concentration and distribution of the plumes in the small scale at a quasi-steady state. Finally the vertical profiles of the plumes are shown. This data has also been made available to partners in a netCDF format to link between models and various imaging systems.

Bubble plumes

The effects of ocean current on bubble plume development are investigated as shown in Figure 17 and Figure 18.

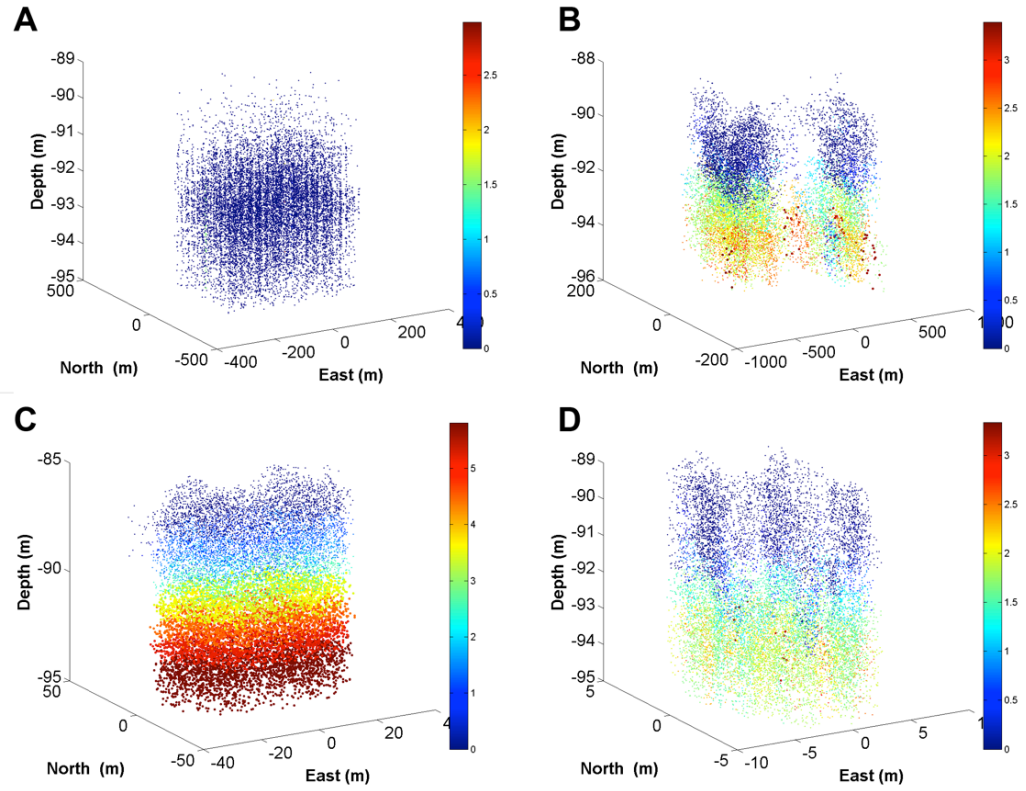

Figure 17: Bubble plume (by d_{eq}) scenarios with no ocean current input, showing formations for the Chimney reactivation (A), Elongated conduit (B), Blowout (C) and Leaky well (D).

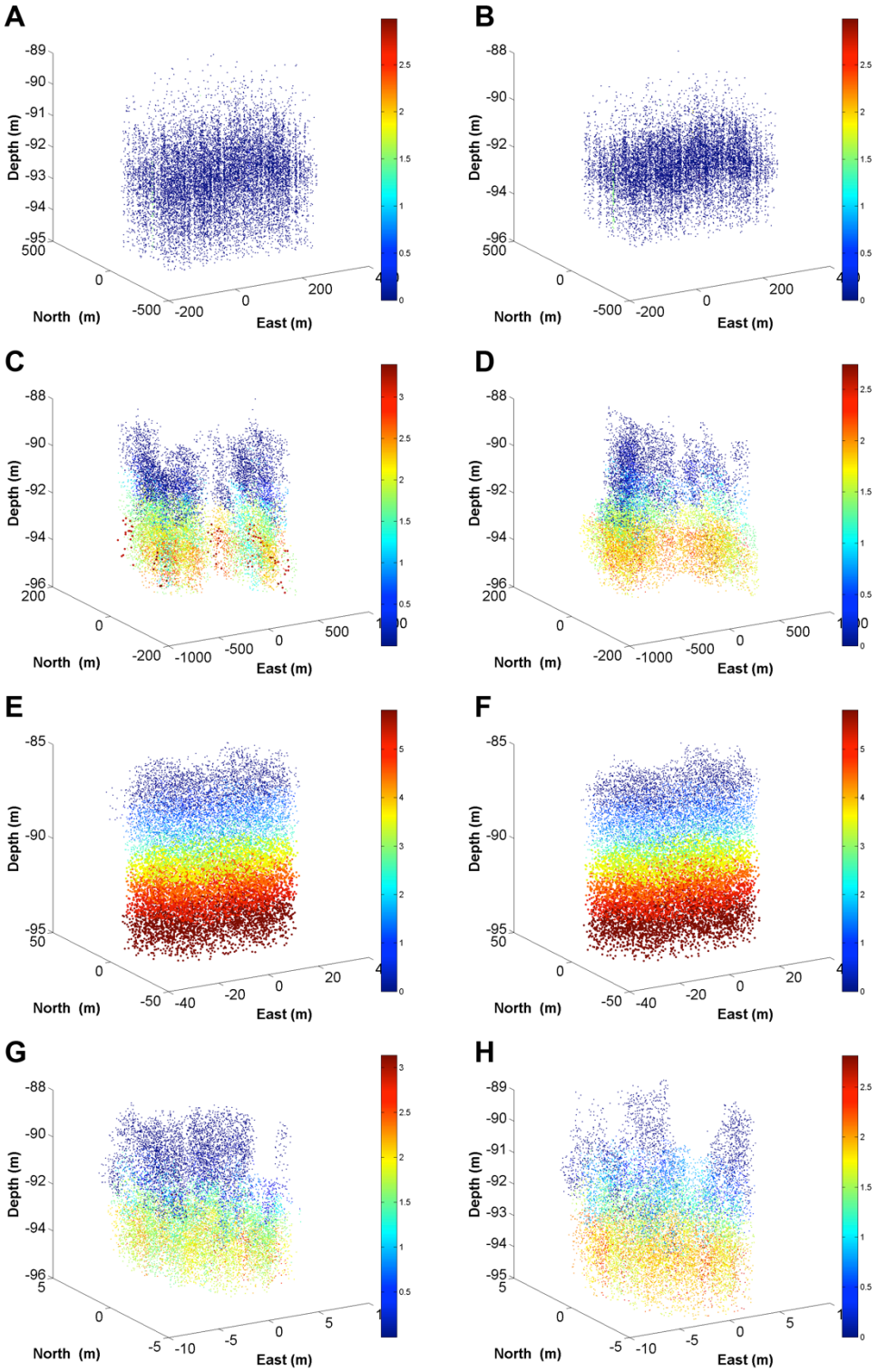

Figure 18: Bubble plume (by d_{eq}), showing formations for the Chimney reactivation (A, B), Elongated conduit (C, D), Blowout (E, F) and Leaky well (G, H). The first column has a minor ocean current input from the BOM and the second column has a majors ocean current from the BOM.

What can be seen from the bubble plumes during a chimney reactivation is that the larger bubbles are of a low quantity (being released randomly from different pockmarks within the leakage area). This is due to the low leakage flux (although high leakage rate) meaning that there is only a small amount of large bubbles being visible, at any given time, however the rest of bubbles dissolving left over from previous pockmarks mean that there is a large quantity of small bubbles that remain. This bubble plume has been observed in field experiments such as the QICS experiment, or from natural leakage plumes when there are intermittent leakages from a number of pockmarks.

Due to the greater leakage flux, the remainder of the scenarios have an equal distribution of bubbles across the set leakage area. The maximum bubble size in each scenario is 6.4mm calculated using the theories of bubble instability (Eq. 9), however, due to use of bubble distribution, and the Eurlerian method for the plume simulations causing the bubble size to appear closer to the mean diameter. A main point to note is the lack of change in the bubble plumes with the current between the left and right hand columns (Figure 18) in the major and minor current scenarios.

Footprint – DIC and pH.

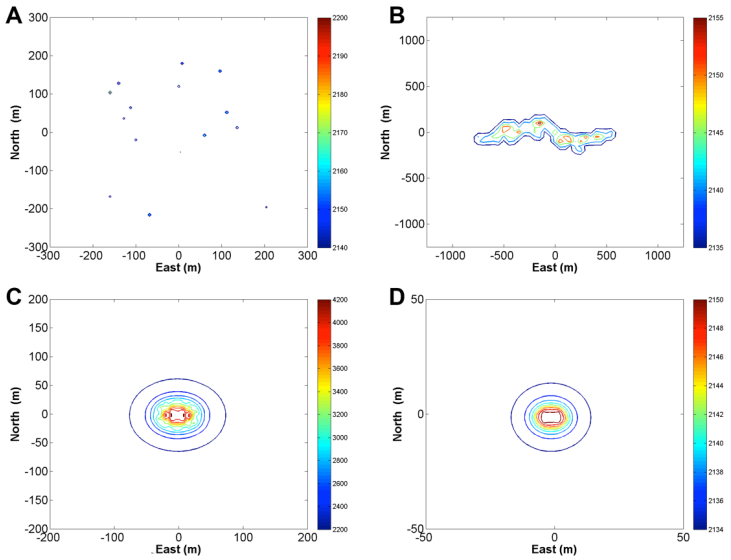

Figure 19: DIC (µmol/m^3) on the seabed, showing formations for the Chimney reactivation (A), Elongated conduit (B), Blowout (C) and Leaky well (D).

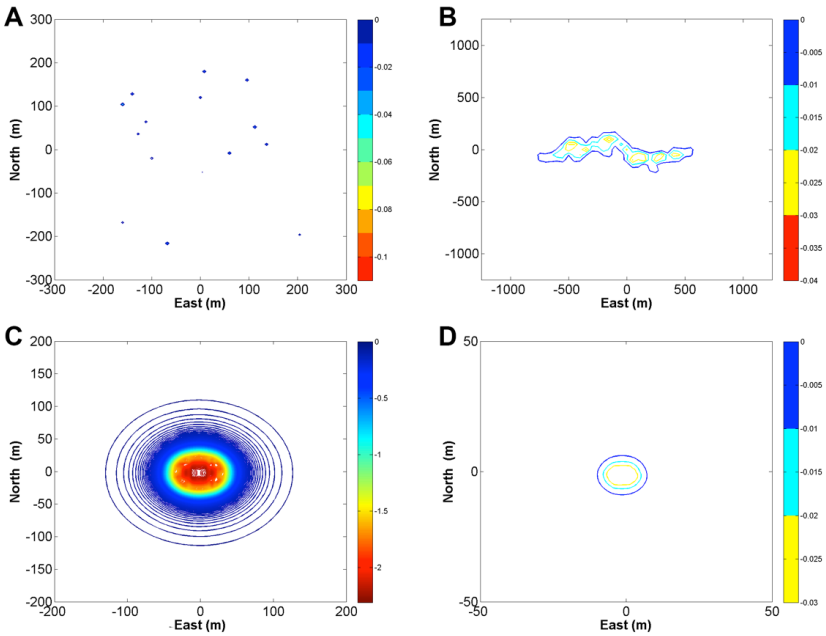

Figure 20: pH change on the seabed, showing formations for the Chimney reactivation (A), Elongated conduit (B), Blowout (C) and Leaky well (D).

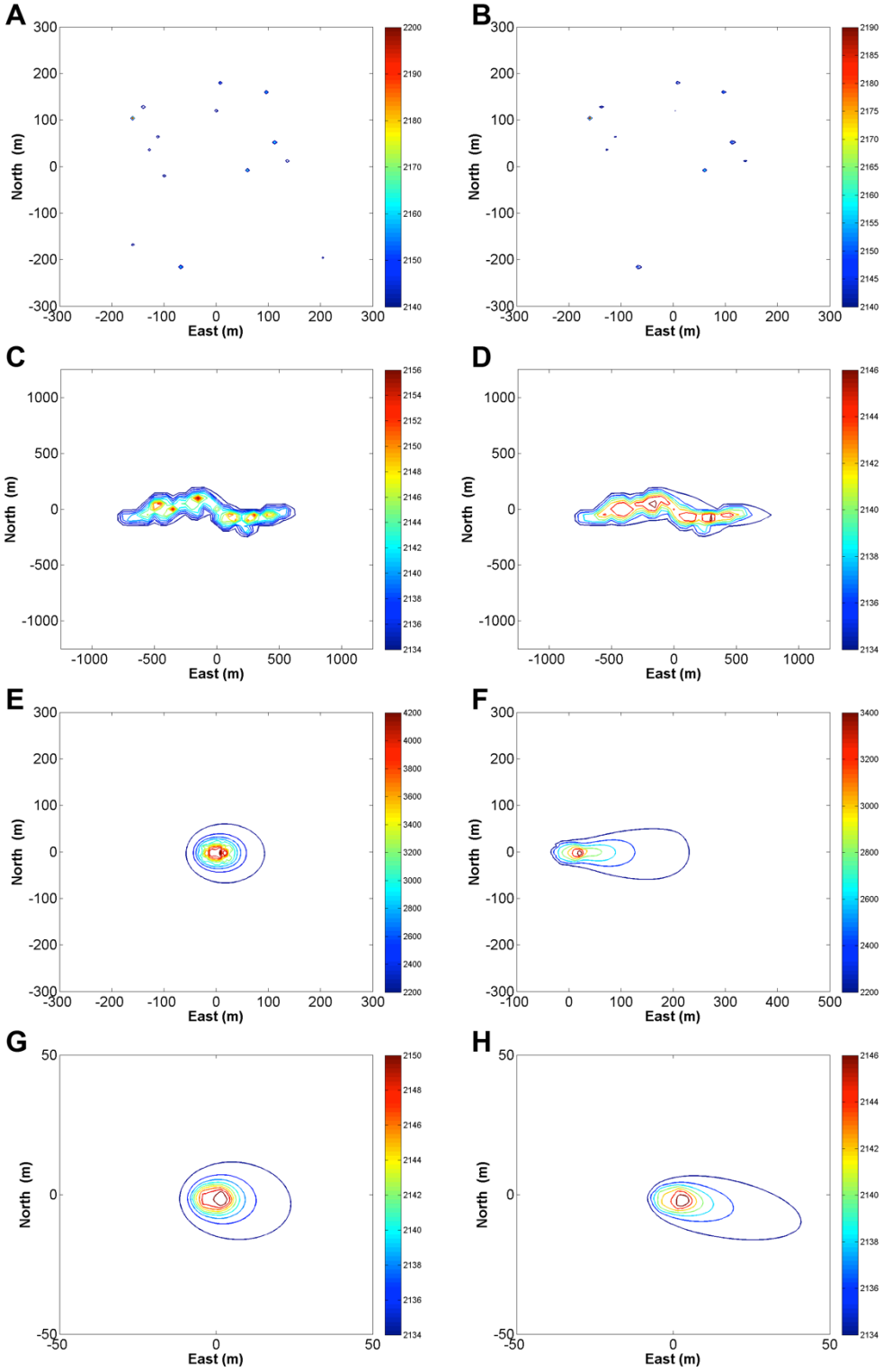

Figure 21: DIC (µmol/m^3) on the seabed, showing formations for the Chimney reactivation (A, B), Elongated conduit (C, D), Blowout (E, F) and Leaky well (G, H). The first column has a minor ocean current input from the BOM and the second column has a major ocean current from the BOM.

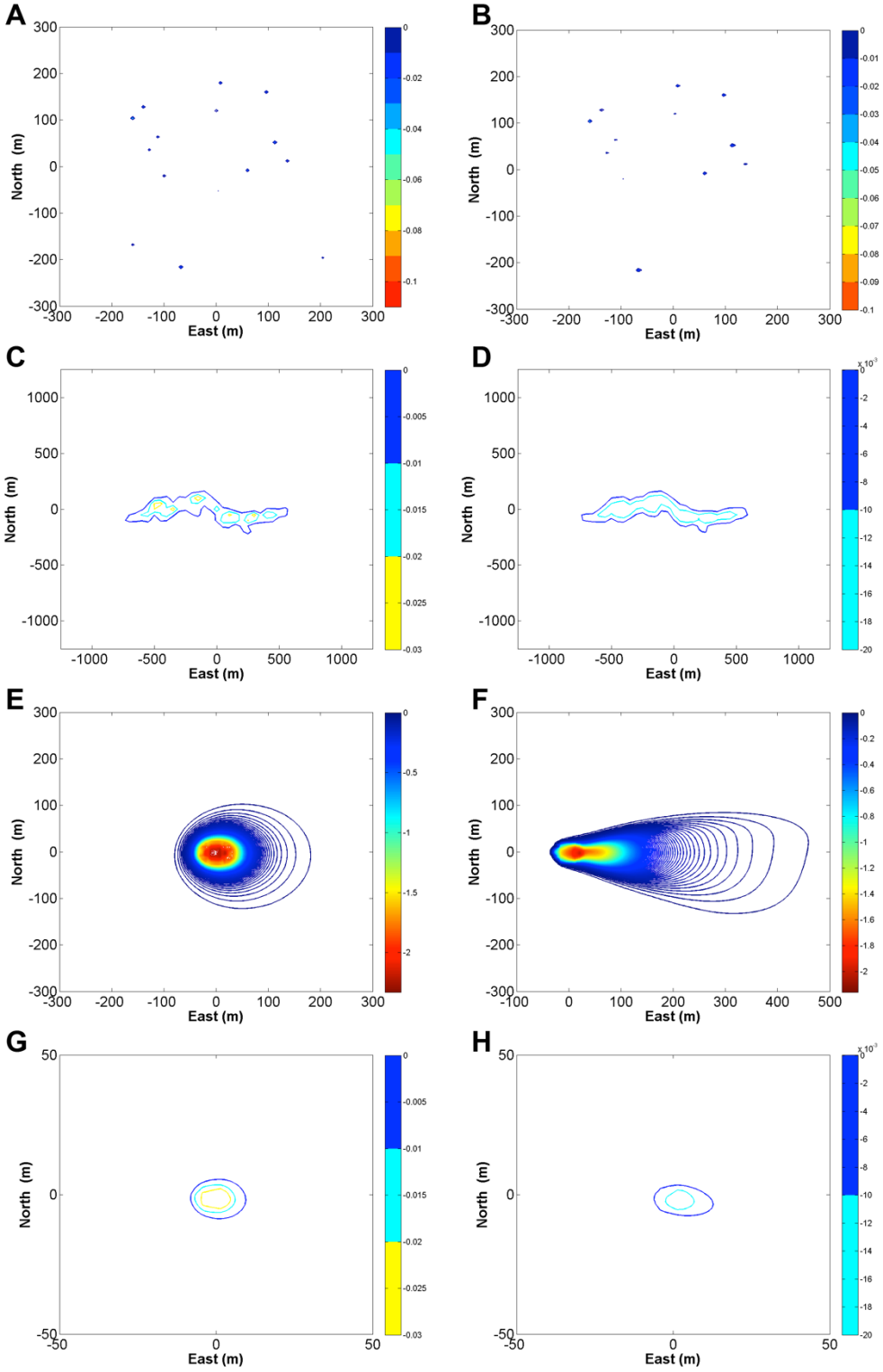

Figure 22: pH change on the seabed, showing bubble formations for the Chimney reactivation (A, B), Elongated conduit (C, D), Blowout (E, F) and Leaky well (G, H). The first column has a minor ocean current input from the BOM and the second column has a major ocean current from the BOM.

From the above DIC and pH results, it can be seen that changes from the background vary depending on the scenario. The scenarios with the greater leakage flux provide the greatest changes in DIC and those scenarios with the larger areas dilute the changes in DIC. The current can be seen to have an effect, by reducing the maximum change in DIC. However, this enlarges the areas affected by a smaller change.

As the DIC is linked to pH, similar effects are expected to be seen in the corresponding pH countour plots, where the smallest contour highlights a pH change of 0.01.

Vertical and mean profiles – Dissolved mass, normalized against the source flux

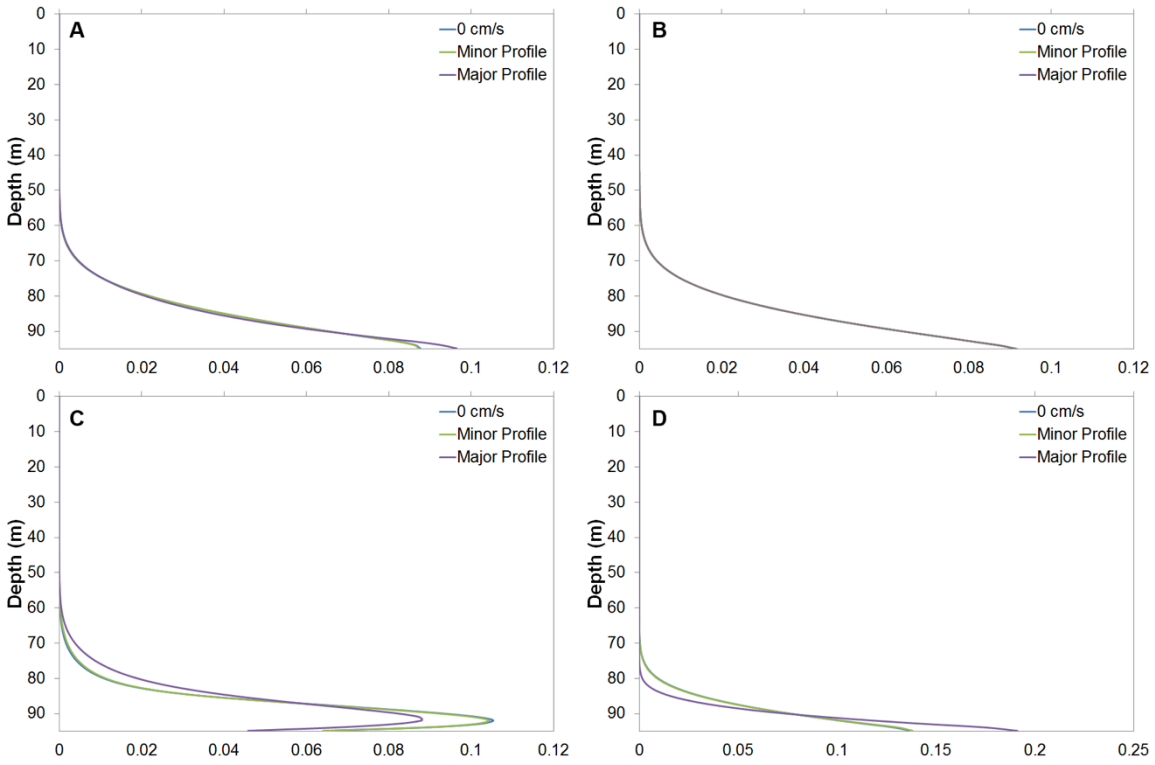

Figure 23: normalised vertical profile of dissolved mass (kg/kg_{total}), for the Chimney reactivation (A), Elongated conduit (B), Blowout (C) and Leaky well (D), showing data for no ocean current input, the minor ocean current input from the BOM, and the major ocean current from the BOM.

It is indicated from Figure 23 that although the profiles for each scenario are similar, when a larger current occurs, a greater proportion of the leaked CO_2 dissolves and remains in the

bottom layers, where the lower current (and no current scenarios) have a slightly greater vertical distribution. Without current or in the case of minor current, the CO_2 enriched seawater generally remains in the area where CO_2 bubbles leak, which provide a relatively large background CO_2 concentration, therefore decreasing the dissolution rate and leading the increase in vertical height of CO_2 solution plume.

The exception is in the blowout case, where the up flow from the high bubble void fraction provides a vertical momentum, moving the dissolved CO_2 plume from the seabed. A greater mass is also found towards the bottom of the plume with no current due to the plumes with current providing horizontal movement on top of the induced vertical momentum, spreading more of the plume in the horizontal at the top as well as the bottom of the plume.

Discussion

The results reported here are those at a quasi-steady state, where the maximum pH change has been reached, and the distribution is no longer witnessing any significant changes.

Previous studies (Dewar et al., 2013) have shown that the seasonal changes at the leakage depth of ~100m have minimum effect in the small scale. As can be seen from the results show in this report, the ocean current has a minimum effect on the bubble plume formation and dynamics. However, the ocean current has a great effect on the dissolved CO_2 plume, with the larger currents creating a less concentrated change in DIC and pH by spreading it over a larger volume and smaller currents providing the greatest changes but over a minimum volume.

The leakage flux has a larger effect on the strong DIC and pH changes than the leakage rate, where the chimney reactivation with the largest leakage rate provides the smallest changes due to the large area over which this is spread. Hence the blowout with a relatively large leakage rate (2/3 of the chimney reactivation), but over a far smaller area provides the greatest changes in both DIC and pH changes.

The leakage bubble size, determined in general by the structure of sediments (the channel of sediments or the size of the pockmarks), also has a great effect on the plumes, larger diameters take longer to dissolve and will therefore spread the dissolution over a larger vertical volume providing a less pH (or DIC) change in the waters. Therefore it is essential for monitoring or detecting of the CO_2 leakage to measure the bubble/droplet size.

GCM regional modelling results

In addition to study the natural current variability the Bergen Ocean Model has been used to simulate larger scale transport of the CO_2 consentration. The resolution of the BOM set-up is 800 meters. Under the assumption that the CO_2 signal is dilluted enough to not influence on the seawater density the consentration can be simulated as a passive tracer in on this scale.

As source of CO_2 the vertical profiles provided by the HWU model has been used. Apart for the passive tracer, the setup is similart to the one being used to study environment statististics as describe earlier and in ECO2 D3.3.

Since this model includes current variability that is believed to be representative for the area, it can be used to study how the CO_2 signal varies in time. Table 4 shows the mean consentration at the seafloor and in the location of the leak for the different scenarios.

Table 4 The mean concentration and the standard deviation in the source grid cell.

Scenario	Mean concentration $\mu mol/kg_{sw}$	Standard deviation $\mu mol/kg_{sw}$
Blowout-20cms	22.7	9.8
Blowout-Maj	19.8	8.4
Chimney-20cms	36.04	21.4
Chimney-Maj	34.86	16,6
Leaky_Well-20cms	0.02	0.01
Leaky_Well-Maj	0.02	0.01

Considering the background concentration in the ocean being of the order of 2000$\mu mol/kg_{sw}$ the signal even at the source grid cell is 1% in magnitude.

To illustrate the time variability Figure 24 and Figure 25 show the mean concentrations, and corresponding standard deviations, for the Blowout and Chimney scenarios.

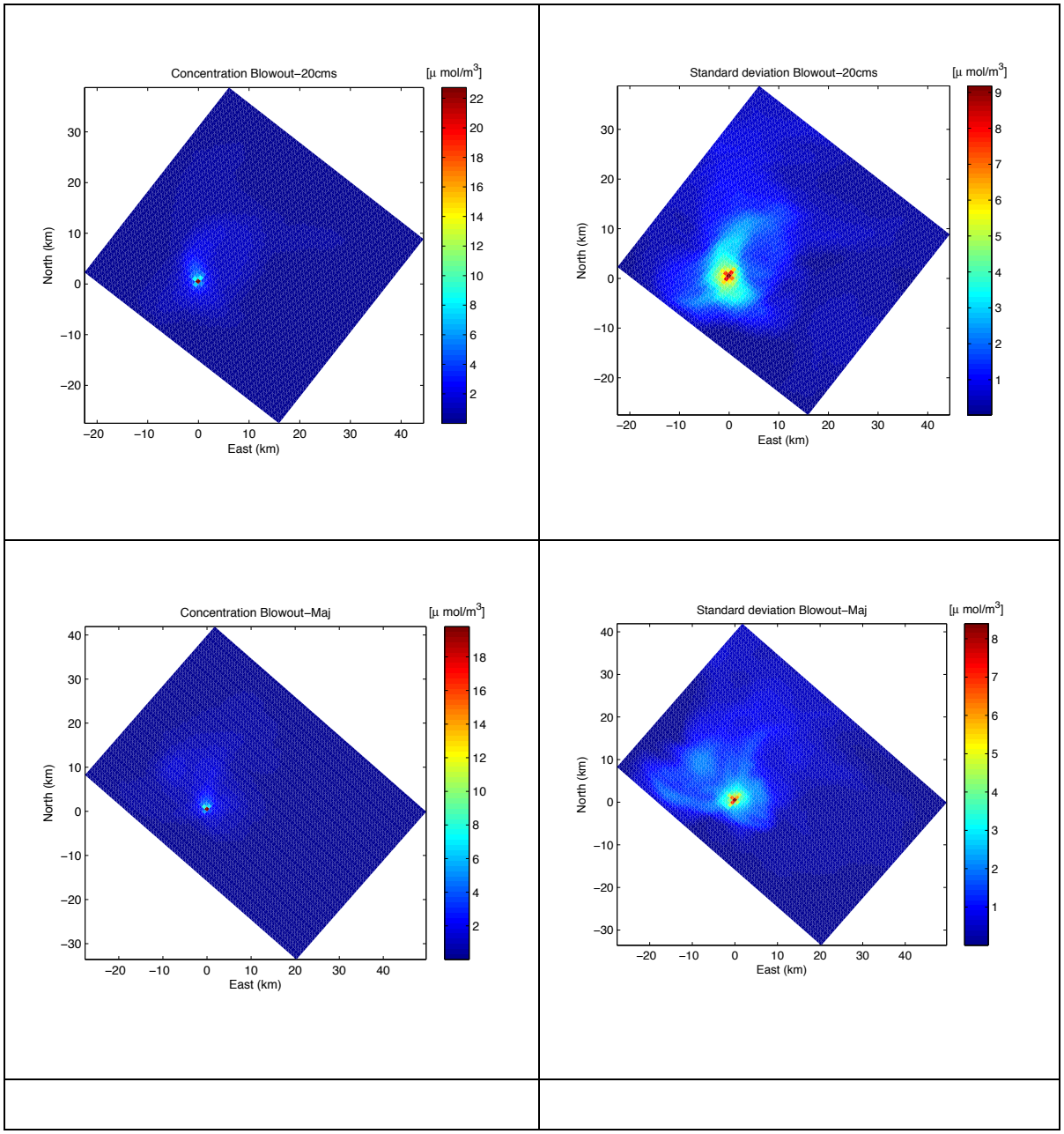

Figure 24: Mean (left) and standard deviation (right) concentrations at the seafloor for the Blowout scenarios. Notice the difference in values for the colour contours.

The source grid cell is easily identified in all scenarios, and as expected, the mean CO_2 signal is highly localized to the vicinity of the leak. However, the variability of the signals show spatial structures, indicating that even away from the source patches of higher CO_2 concentration can be expected. Even if these patches will be very temporal, and most

likely will not impose any long-term environmental impact, they might increase our ability to detect a leak.

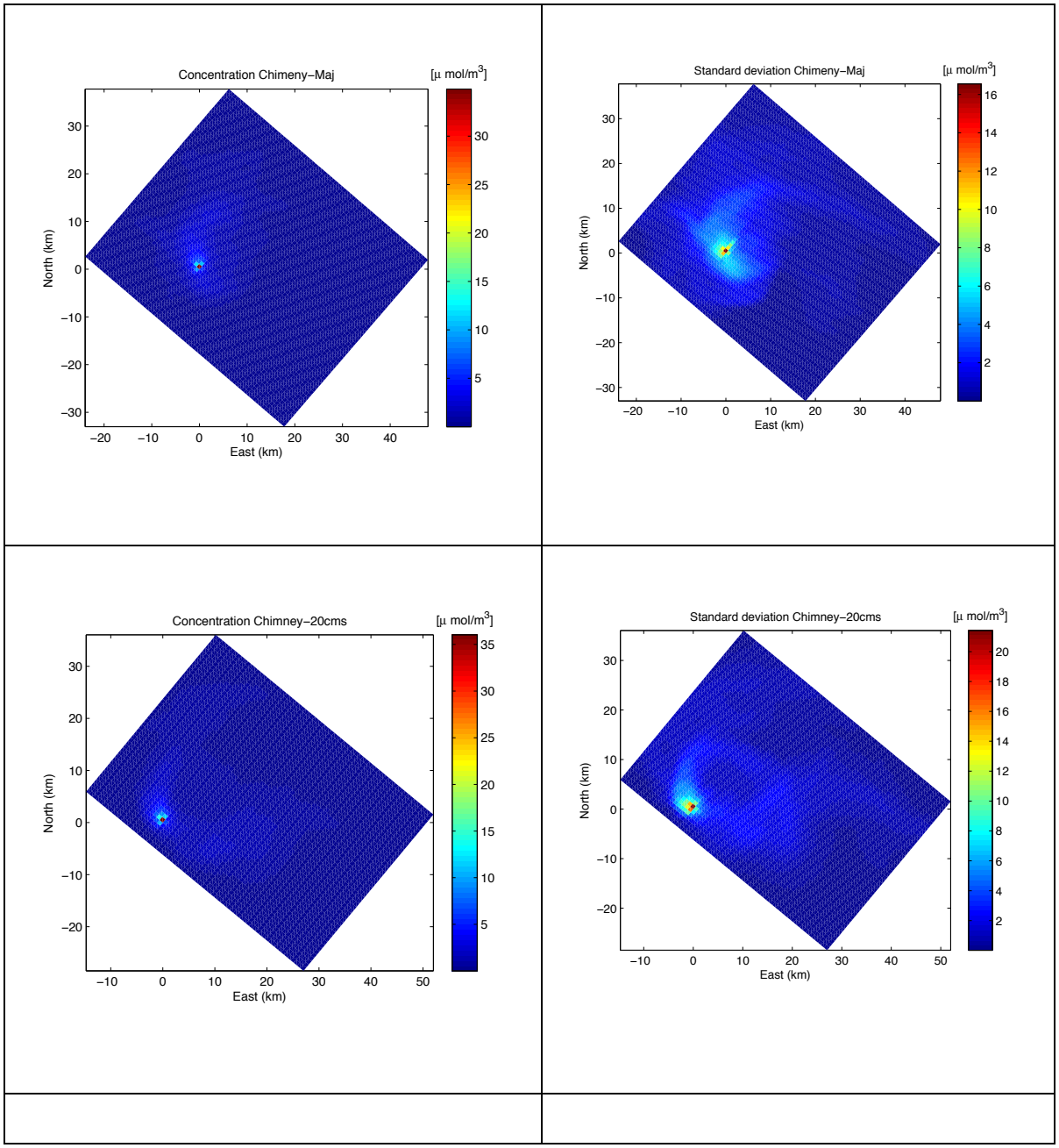

Figure 25: Mean (left) and standard deviation (right) concentrations at the seafloor for the Chimney scenarios. Notice the difference in values for the colour contours.

As further illustration cumulative probability distributions of CO_2 concentration for the Chimney-Maj scenario are shown in Figure 26. At the source the concentration stays above 10 µmol/kg_{sw} almost 100% of the time, while it stays above 40µmol/kg_{sw} 20% of the time. Moving away from the source these values decreases quickly, (Figure 26), but still it reaches 10µmol/kg_{sw} 10% of the time.

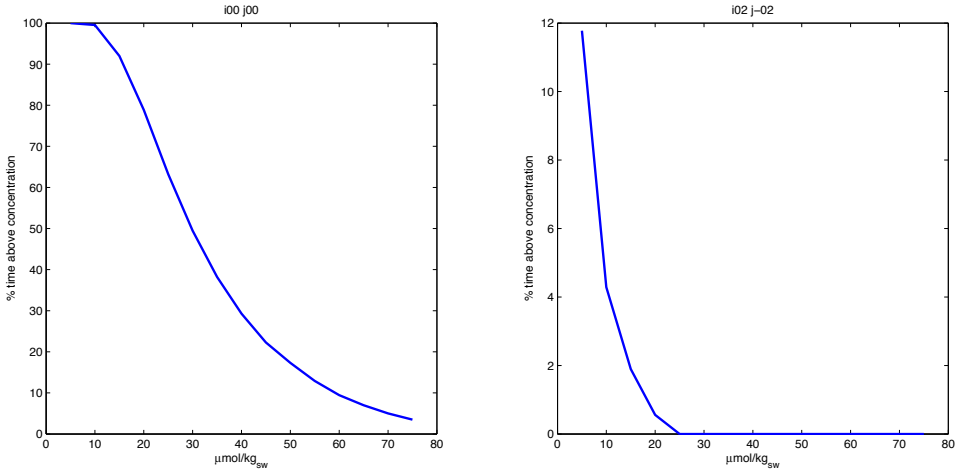

Figure 26 For the Chimney-Maj scenario: % of time the concentration stays above the values on the x-axis. Left: At the source grid cell, right moving two grids cell in the positive x-direction and two grid cells in negative y-direction. All values taken at the seafloor.

Figure 27 shows the vertical profile of the cumulative distribution at the source, still for the Chimney-Maj scenario. At the seafloor the concentration stays above 15µmol/kg_{sw} 90% of the time, while the similar concentration is approximately 8µmol/kg_{sw} 10 meters above the seafloor. The CO_2 signal never reaches at 25-30 meter above the seafloor.

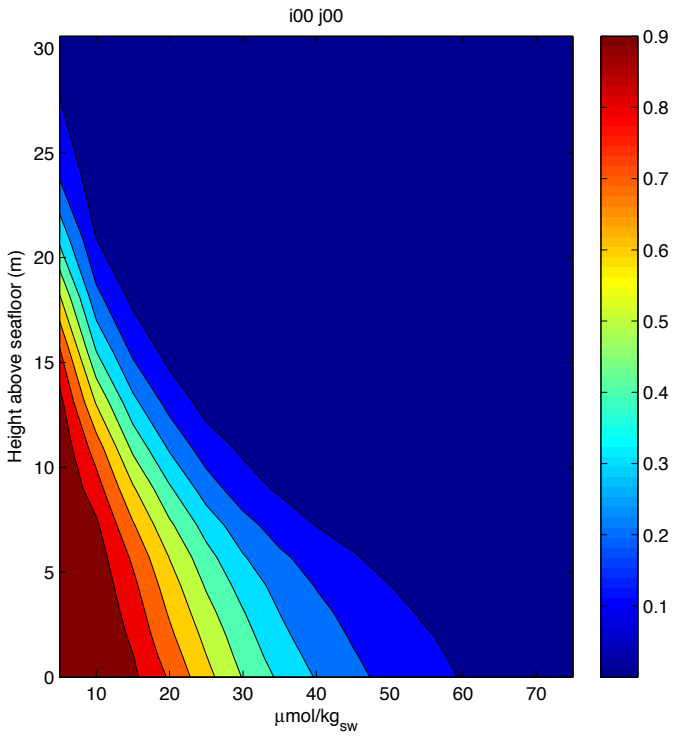

Figure 27: Vertical profile of the relative time the concentration stays above the value on the x-axis. At the source and for the Cimney-Maj scenario.

References

Boudreau, B.P., 1997. Diagenetic models and their implementation: modelling transport and reactions in aquatic sediments. Springer

Bolding K, Burchard H, Pohlmann T, Stips A: Turbulent mixing in the Northern North Sea: a numerical model study. *Continental Shelf Research*, 2002, 22:18-19

Botnen, HA, Omar AH, Thorseth I, Johannessen T, Alendal G**.** (2014). The effect of submarine CO2 vents on seawater: Implications for detection of subsea carbon sequestration leakage. Accepted in *Limnology & Oceanography*.

Bozek, Y., Thomas, H., Schiettecatte, L.S., Borges, A.V., Elkalay, K., de Baar, H.J.W., 2006. Assessment of the processes controlling seasonal variations of dissolved inorganic carbon in the North Sea. *Limnol. Oceanogr*., 51, 2746–2762, doi:10.4319/lo.2006.51.6.2746.

Bruggeman, J., Bolding, K.: A general framework for aquatic biogeochemical models. *Environmental Modelling & Software*. 2014. http://dx.doi.org/10.1016/j.envsoft.2014.04.002

Davies, A. M., & Furnes, G. K. (1980). Observed and computed M2 tidal currents in the North Sea. *Journal of Physical Oceanography*, *10*(2), 237–257. doi:10.1175/1520-0485(1980)010<0237:OACMTC>2.0.CO;2

Dewar M, Chen B, Evgeniy Y, Avlesen H., Alendal G, Ali A., Vielstädte L. Technical report on verified and validated application of droplet/ bubble plume-, geochemical- and general flow- models. ECO2 (project number: 265847)deliverable 3.3 to the Commission, November 2013.

Duan, Z., sun, R., Zhu, C., Chou, I.M.,2006. An improved model for the calculation of CO_2 solubility in aqueous solutions containing Na+, K+, Ca2+, Mg2+, Cl-, and SO42-. *Marine Chemistry* 98, 131-139.

Duan, Z., Moller, N., Weare, J.H., 1992. An equation of state for the CH_4–CO_2–H_2O system: I. Pure systems for 0 to 1000 °C and 0 to 8000 bar. *Geochim. Cosmochim. Acta* 56, 2605– 2617.

ECO2 Deliverable 4.1: Report on marine communities. July 2014. Ana M Queirós1, Karl Norling2, Teresa Amaro2, Joana Nunes1, Denise Cummings1, Eugenio Rastelli, Evgeny Yakushev2, Kai Sorensen2, Carolyn Harris1, Malcom Woodward1, Roberto Danovaro, Elisabeth Alve4, M. MolariX, S. GrünkeX, M. WeberX, K. GuiliniX, N BigalkeX, F. WenzhöferX, Doung de BeerX, A. RametteX, C. De VittorX, A. VanreuselX, A. BoetiusX and Stephen Widdicombe1. 2014 Potential impact of CCS leakage on marine communities. ECO2 Deliverable 4.1: Report on marine communities. July 2014.

Geng, M., Duan, Z.H., 2010. Prediction of oxygen solubility in pure water and brines up to high temperatures and pressures. *Geochimica et Cosmochimica Acta* 74, 5631-5640.

Graham A., Omar A., Alendal G., Pedersen R.B., Johannessen T., Yakushev E., Widdicombe S., Diepenbroek M., Janbu A.D., Sollie O.K., Eggen S. 2014. CO2 Base. Preparing for sub-sea storage of CO_2: Baseline gathering and monitoring for the North Sea. Step I: Planning the survey. Report. Project No: 806748. Uni Research AS

Mao, S., Duan, Z.H., 2006. A thermodynamic model for calculating nitrogen solubility, gas phase composition and density of the N2-H2O-NaCl-system. *Fluid Phase Equilibria* 248, 103-114.

Pawlowicz, R., Beardsley, B., & Lentz, S. (2002). Classical tidal harmonic analysis including error estimates in MATLAB using T-TIDE. *Computers & Geosciences*, *28*(8), 929–937. doi:10.1016/S0098-3004(02)00013-4

Salt LA, Thomas H, Prowe AEF, Borges AV, Bozec Y and de Baar HJW.(2013). Variability of North Sea pH and CO_2 in response to North Atlantic Oscillation forcing. *J. Geophys. Res.: Biogeosciences,* **118,** 1–9, doi:10.1002/2013JG002306

Wüest, A., N. H. Brooks, and D. M. Imboden (1992), Bubble plume modeling for lake restoration, *Water Resour. Res.,* 28(12), 3235–3250, doi:10.1029/92WR01681.

Yakushev E.V., Pollehne F., Jost G., Umlauf L., Kuznetsov I., Schneider B. 2007. Analysis of the water column oxic/anoxic interface in the Black and Baltic seas with a Redox-Layer Model. *Marine Chemistry*, 107, 388-410

Yakushev E., Protsenko E. 2014. Varying redox conditions in benthic biogeochemistry: simulations with Bottom ReDox Model (BROM). *Geochemical Transactions* (submitted)

Zheng, L., Yapa, P.D., 2002. Modeling gas dissolution in deepwater oil/gas spills. *J. of Marine Systems* 31, 299-309.